Damping reduction factors for adjacent buildings connected by fluid-viscous dampers

Michele Palermo *[(1)], Stefano Silvestri [(2)]

[(1)] Assistant professor, Department of Civil, Chemical, Environmental and Materials Engineering, University of Bologna, Italy. *Corresponding author.
[(2)] Associate professor, Department of Civil, Chemical, Environmental and Materials Engineering, University of Bologna, Italy.

This work investigates the dynamic behaviour of a multi-storey frame building, assumed as the structure to be controlled, connected with an adjacent support structure by means of horizontal fluid viscous dampers. The dampers connection system has two main effects: (i) energy dissipation provided by the viscous dissipative forces, (ii) energy transfer between modes leading to modes coupling effects between the two buildings without a significant dissipation of energy. The relative contribution of the two effects is highly dependent on the main properties of the coupled system. To investigate this complex behaviour, first the minimal coupled dynamic system composed by two Single-Degree-Of-Freedom systems connected by a viscous damper is analysed. The theory of complex damping is used to determine complex frequencies and damping ratios, while analytical expressions of steady state response under harmonic excitation are determined to investigate the influence of the system parameters on the maximum dynamic amplifications. The seismic response is also investigated through a wide parametric study with the aim of evaluating the trends of the damping reduction factors with respect to the main dynamic parameters of the coupled system. Minimum values of the damping reduction factors and corresponding optimal damping coefficients are determined. Then, the analyses are extended to uniform multi-storey structures for which minimum damping reduction factors are provided for a wide range of the key system parameters. Comparisons between one-storey and uniform multi-storey systems are provided. The results can be useful for a preliminary design of the dampers connection system and for the evaluation of its effectiveness based on the fundamental dynamic properties of the connected buildings.

KEYWORDS
Adjacent buildings; Viscous dampers; Energy dissipation; Energy transfer; Seismic response; Damping reduction factors.

1. Introduction

Connecting adjacent buildings through dissipative devices can be an effective solution for mitigating the dynamic response under seismic excitation and reducing the possibility of poundings, which cannot be ignored as demonstrated by reconnaissance after major seismic events such as 1985 Mexico City and 1989 Loma Prieta earthquakes [1-4]. Scientific research developed in the last decades include both theoretical studies and experimental research.

Theoretical studies were mainly focused on the identification of optimal viscous dampers by mean of stochastic analyses and optimization procedures. Luco et al. 1998 [5] investigated the response to harmonic motion at the

base of two adjacent structures of different height modelled as uniform, elastic, continuous shear beams and identified optimal damping values minimizing the top storey response of the taller structure near the first and second mode. Xu et al. 1999 [6] and Zhang and Xu 2000 [7] investigated the dynamic response of multi-storey adjacent buildings modelled as shear-type systems and connected through viscous dampers by using the pseudo-excitation method for handling non-classical damping properties of the system. Aida et al. 2001 [8] investigated the dynamic behaviour of two Single-Degree-Of-Freedom systems connected by a Kelvin-Voigt damper and proposed an approximate tuning for optimal modal damping ratios. A similar study was conducted by Zhu and Xu 2005 [9] to determine optimum parameters for a Maxwell damper connecting two Single-Degree-Of-Freedom systems. Kim et al. 2006 [10] investigated the effect of installing viscoelastic dampers in places such as seismic joints or building-sky-bridge connections to reduce earthquake-induced structural responses. Bhaskararao and Jangid 2006 [11] investigated the seismic behaviour of adjacent buildings connected through friction dampers, considering both dampers with uniform distribution of slip forces along the height and dampers with different slip forces along the height. Results showed that friction dampers can be very effective in reducing the earthquake response of two adjacent buildings. In 2007 the same authors [12] derived closed form expressions in terms of the mass and frequency ratios of two connected structures for the optimum damper coefficient leading to minimum relative displacements and absolute accelerations under harmonic excitation, as well as minimum mean square responses under stationary white-noise random excitation. Zhu et al. 2011 [13] introduced a reduced order model to obtain analytical formulas for optimum parameters of visco-elastic dampers connecting adjacent multi-storey buildings for different optimization criteria. Gattulli et al. 2013 [14] investigated the complex eigenvalues of two SDOF systems connected by a visco-elastic damper through parametric studies aimed at determining optimal damper design parameters and design charts for preliminary design of dampers. Tubaldi et al. 2014 [15] investigated the probabilistic response of two adjacent steel structures connected with linear and non-linear visco-elastic dampers accounting for the uncertainties associated to both the seismic input and the model parameters. The results indicated that the performances of the systems are more sensitive to the viscous properties than to the stiffness properties of the dampers. In 2015 Tubaldi [16] analysed the dynamic behaviour of two adjacent buildings of different height connected by a single viscous/viscous-elastic damper at the top storey of the lower building through an analytical continuous model. Parametric analyses were conducted to evaluate the dependence of the natural frequencies and damping ratios on the main system parameters. In 2016 Kasagi et al. [17] investigated the effect of damper non-linearity on the connecting devices considering both high-damping rubber dampers and oil dampers with and without relief mechanism. Results showed that while high-damping rubber dampers are effective at a rather small deformation level, oil dampers without relief mechanism are effective at a larger deformation range. In 2017 Kandemir-Mazanoglu and Mazanoglu [18] proposed an optimization procedure for optimum location and capacity of linear and non-linear viscous dampers to prevent pounding effects.

Few experimental investigations have been conducted in the last decades to assess the performances of adjacent buildings connected by dissipative devices. Xu et al. 1999 [19] conducted experimental tests on two 3-storey shear buildings with different natural frequencies connected by fluid dampers and subjected to unidirectional harmonic excitation. The two buildings without fluid dampers were first tested to obtain their individual dynamic properties. Then, tests were carried out on the two buildings connected by fluid dampers of different damping coefficients to determine modal damping ratios**.** Yang et al. 2003 [20] carried out experimental tests on scaled five-storey and six-storey steel frames connected by fluid viscous dampers. The experimental results showed that the installation of fluid dampers of proper parameters could significantly increase the modal damping ratios and reduce the seismic responses of both buildings, while the natural frequencies of both buildings remained almost unchanged. The seismic performances of adjacent buildings linked by fluid dampers were much superior to those of the adjacent buildings linked by rigid rods.

In the past, the dynamic behaviour of frames equipped with linear viscous dampers leading to a Mass Proportional Damping (MPD) system was investigated by Trombetti and Silvestri 2004 [21]. The results

indicated that the MPD system, among the classically damped systems, is the one providing the best overall performances in terms of minimum top-storey response variance to a Gaussian band limited white noise input. Then, a practical solution to implement an "approximate" MPD system was proposed by connecting the reference building to an adjacent stiff support structure, such as a reinforced concrete core or a braced frame. It was found that the solution leads to seismic performances similar to those offered by the "exact" MPD system (Trombetti and Silvestri 2007 [22]).

In this work, a comprehensive study is developed with the aim of evaluating the effectiveness of connecting two adjacent multi-storey buildings with linear viscous dampers at all floors. The dynamic properties of the coupled system and its dynamic response to harmonic and seismic excitation are investigated. In particular, trends of the displacement damping reduction factors are obtained as function of both the dampers properties and key dynamic parameters of the two structures. The results can be used for the preliminary design of the added dampers connection system.

2. Problem statement and parametric study

2.1. Assumptions and objectives

Two adjacent multi-storey structures connected through horizontal fluid-viscous dampers at all floors are considered in the present study. The following assumptions are introduced so that the problem can be handled with an analytical approach:

- The two adjacent structures are symmetric in plan, with their symmetry plan in the same alignment.
- The dynamic input is applied along the direction of the symmetry plan.
- Since the two buildings are close to each other, the same input is applied at the base of both buildings.
- The two adjacent buildings have the same number of storeys, equal to N, and uniform inter-storey height h.
- Each building is modelled as a shear-type frame structure, with lumped mass at each floor level. The frame elements are assumed to remain in the elastic range.
- Equal viscous dampers are located at all floors, each one connecting the two buildings at the same storey.
- A linear force-velocity relationship is assumed for the viscous dampers.
- The axial stiffnesses of the connection system through which the damper is installed and of the fluid viscous damper itself (flexibility associated to oil compressibility) are large enough so that each damper can be modelled with a purely linear viscous dashpot model (representing the limiting case of the Maxwell model with a spring of infinite axial stiffness, Castaldo and De Iuliis 2014 [23], Silvestri et al. 2010 [24]). According to this constitutive model, the damping force is proportional to the relative velocity between the neighbour floors of the two structures.

Under these assumptions a two-dimensional system like the one represented in Figure 1 can be analysed. Hereafter, the system composed by the two buildings connected through the viscous dampers (Figure 1a) will be also referred to as N-storey coupled system, while the single buildings will be also referred to as the "reference" building (or, alternatively, Building 1) and the "support" building (or, alternatively, Building 2). The reference structure is intended as the building to be controlled by the supplemental dampers system that utilizes the other building as support. Furthermore, for comparison purposes, also two MPD systems corresponding to Building 1 and Building 2 will be analysed. Each MPD system is composed by one of the two buildings linked with horizontal dampers connected to fixed points (Figure 1b). For each MPD system,

the damping coefficient of the damper located at the *i*-th storey is proportional to the corresponding *i*-th floor mass.

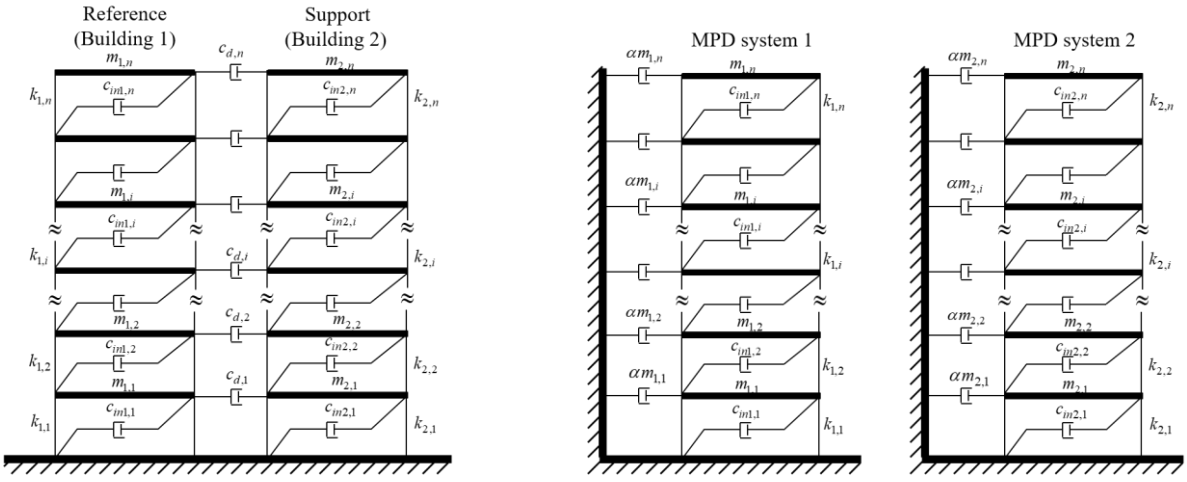

(a) (b)

Figure 1: The coupled *N*-storey system (a) and the corresponding MDP systems (b).

The main objective of this work is to investigate the energy dissipation capabilities of the connection system made of supplemental viscous dampers with a specific focus on the damping reduction factor of the peak seismic displacement response of the reference building, as compared with the limiting case of the same building equipped with a MPD system. For this aim, a comprehensive parametric study has been conducted, starting from one-storey systems and then moving to multi-storey systems. For the one-storey systems, the complex frequencies and corresponding damping ratios are evaluated according to the theory of complex damping and compared with those of the corresponding disconnected buildings, as obtained from classical modal analysis. The steady state response under harmonic input at the base is then investigated to obtain frequency response curves (Chopra, 2001 [25]) and surfaces. The seismic response is also investigated with the purpose of evaluating the trends of the displacement damping reduction factors with respect to the key dynamic parameters. Finally, the analyses are extended to multi-storey systems with the main purpose of evaluating the trends of the damping reduction factors of the peak roof displacement. The study is focused uniquely to displacement reduction factors since they can be used directly for design purposes to reduce the ordinates of the reference 5%-damped pseudo-acceleration spectrum, thus obtaining the corresponding design elastic spectra for large damping ratios.

2.2. The equation of motion and the dynamic analyses

The dynamic behaviour of the *N*-storey coupled system under earthquake excitation is governed by the following equation of motion:

$$\mathbf{M}\ddot{\mathbf{u}} + \left(\mathbf{C}_I + \mathbf{C}_D\right)\dot{\mathbf{u}} + \mathbf{K}\mathbf{u} = -\mathbf{M}\mathbf{1}\ddot{u}_g \tag{1}$$

where:

u is a 2*N*-dimensional horizontal relative displacement vector (with respect to ground displacement u_g). The first *N* components of **u** (from 1 to *N*) collect the horizontal relative displacements of Building 1, while the

remaining N components (from N+1 to 2N) refer to Building 2. $\mathbf{M}=\begin{bmatrix}\mathbf{M}_1 & \mathbf{0}\\ \mathbf{0} & \mathbf{M}_2\end{bmatrix}$, $\mathbf{K}=\begin{bmatrix}\mathbf{K}_1 & \mathbf{0}\\ \mathbf{0} & \mathbf{K}_2\end{bmatrix}$, $\mathbf{C}_I=\begin{bmatrix}\mathbf{C}_{I1} & \mathbf{0}\\ \mathbf{0} & \mathbf{C}_{I2}\end{bmatrix}$, $\mathbf{C}_D=\begin{bmatrix}\mathbf{C}_d & -\mathbf{C}_d\\ -\mathbf{C}_d & \mathbf{C}_d\end{bmatrix}$ are the 2Nx2N mass, stiffness, inherent damping and added viscous damping matrices, respectively. **1** is the 2N-dimensional unity vector. $\ddot{u}_g$ is the ground acceleration. **0** is a NxN matrix with null elements. $\mathbf{M}_1$, $\mathbf{K}_1$, $\boldsymbol{C}_{I1}$ and $\mathbf{M}_2$, $\mathbf{K}_2$, $\mathbf{C}_{I2}$ are the NxN mass, stiffness and inherent damping matrices of Building 1 and Building 2, respectively. $\mathbf{C}_d=\begin{bmatrix}c_{d1} & & & & \\ & \ldots & & & \\ & & c_{di} & & \\ & & & \ldots & \\ & & & & c_{dn}\end{bmatrix}$ is a N x N diagonal matrix. c_{di} is the damping coefficient of the viscous damper that connects the i-th floor of Building 1 with the corresponding i-th floor of Building 2.

The equation of motion of the two MPD systems (Eq. 2) and of the two disconnected buildings (Eq. 3) are particular cases of the general equation of motion (Eq. 1):

- Equation of motion for the MPD systems:

$$\mathbf{M}\ddot{\mathbf{u}}+\left(\mathbf{C}_I+\mathbf{C}_D{}^*\right)\dot{\mathbf{u}}+\mathbf{K}\mathbf{u}=-\mathbf{M}\mathbf{1}\ddot{u}_g \tag{2}$$

- Equation of motion for the two disconnected buildings (Building 1 and Building 2):

$$\mathbf{M}\ddot{\mathbf{u}}+\mathbf{C}_I\dot{\mathbf{u}}+\mathbf{K}\mathbf{u}=-\mathbf{M}\mathbf{1}\ddot{u}_g \tag{3}$$

where $\mathbf{C}_D{}^*=\begin{bmatrix}\mathbf{C}_d & \mathbf{0}\\ \mathbf{0} & \mathbf{C}_d\end{bmatrix}$ is a matrix with the diagonal components of the $\mathbf{C}_D$ matrix and with null off-diagonal terms.

For the general case (Eq. 1), the damping matrix ($\mathbf{C}_I+\mathbf{C}_D$) of the coupled system is non-proportional, thus the evaluation of its frequencies and damping ratios requires the theory of complex damping. For a generic non-proportionally damped system, the damping matrix provides two different effects: (i) energy dissipation associated to the proportional component of the complex damping matrix through the real damping ratio, and (ii) energy transfer between modes associated to the non-proportional component of the complex damping matrix through the imaginary damping ratio. While the energy associated to effect (i) is transformed from mechanical energy to another type of energy (typically heat energy), the energy associated to effect (ii) is not transformed to another kind of energy but rather transferred between modes thus providing coupling effects between modes. As a consequence of this coupling effect, the undamped frequencies of a non-proportionally damped (or coupled) system are no longer independent on the damping matrix. The interested reader may find a complete exposition of the theory in the NCEER-91-0004 [26] report or in the textbook by Cheng 2001 [27].

The parametric studies on the dynamic properties of the coupled system (section 3.3) and on the harmonic steady state response (section 3.4) as well as the time-history dynamic analyses (sections 3.5 and 4.2) are carried out with an ad-hoc developed MATLAB routine. An ensemble of 10 artificially generated ground motions is considered as seismic input for the parametric study. The artificial ground motions are generated using the software SIMQKE (Gasparini and Vanmarcke 1976 [28]) in order to match the design spectrum according to the Italian building code NTC18 [29] (for an average Peak Ground Acceleration equal to 0.12g).

Each artificial record has a total duration of 20 s, while the duration of the stationary part (starting after 2 s) is of 10 s. The average pseudo-acceleration spectrum of the 10 accelerograms (with 5% damping ratio) is shown in Figure 2a. For the applicative example (section 5.2), the El-Centro S00E record (1940 Imperial Valley Earthquake) is considered. Its pseudo-acceleration response spectrum (with 5% damping ratio) is displayed in Figure 2b.

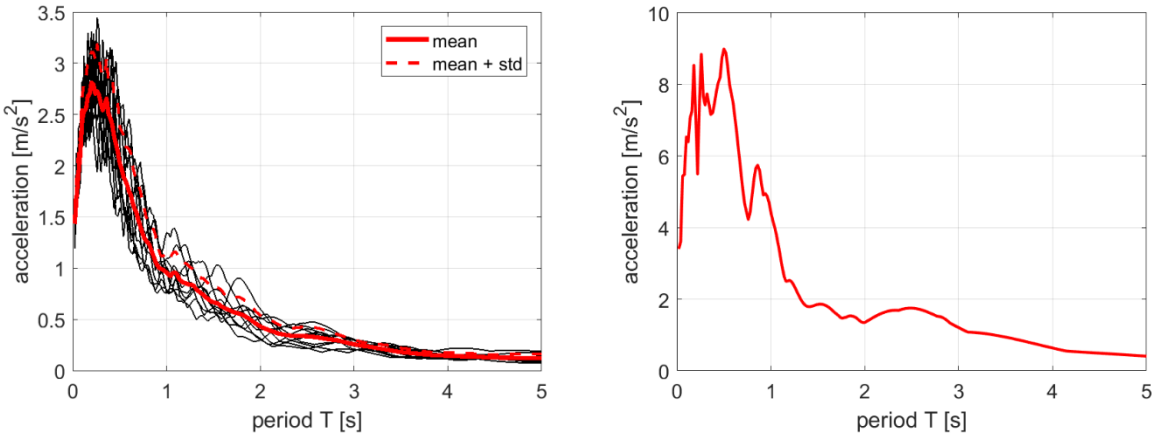

(a) (b)

Figure 2: Pseudo-acceleration response spectra with 5% damping ratio: (a) the ten artificial accelerograms generated with SIMQKE; (b) the El-Centro S00E record.

3. One-storey systems

3.1. Considered systems and key parameters

This section investigates the behaviour of two one-storey adjacent buildings connected through a viscous damper having damping coefficient c_d (Figure 3). Each one-storey building is modelled as a damped Single-Degree-Of-Freedom (SDOF) system with damping coefficient equal to c_{in1} for the SDOF system 1 and c_{in2} for the SDOF system 2. Both c_{in1} and c_{in2} values lead to an inherent damping ratio equal to 5%. The SDOF system 1 is assumed as the reference structure, while the SDOF system 2 is the support structure.

The dynamic response of the coupled one-storey system is compared with those of the corresponding damped SDOF systems, each one having a damping coefficient equal to the sum of the inherent damping (c_{in1} for SDOF system 1 and c_{in2} for SDOF system 2) and the viscous damping of the added damper c_d.

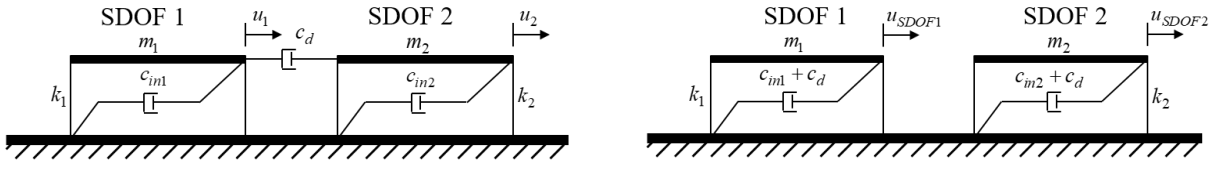

(a) (b)

Figure 3: (a) Coupled one-storey system; (b) SDOF system 1 and SDOF system 2.

The equations of motion of the coupled one-storey system with two degrees of freedom u_1 and u_2 and of the corresponding two damped SDOF systems (having one degree of freedom indicated as $u_{SDOF1}$for SDOF system 1 and u_{SDOF2} for SDOF system 2), as subjected to a ground excitation $\ddot{u}_g$, are given below:

- for the coupled one-storey system:

$$\begin{bmatrix} m_1 & 0 \\ 0 & m_2 \end{bmatrix}\begin{Bmatrix} \ddot{u}_1 \\ \ddot{u}_2 \end{Bmatrix}+\begin{bmatrix} c_{in1}+c_d & -c_d \\ -c_d & c_{in2}+c_d \end{bmatrix}\begin{Bmatrix} \dot{u}_1 \\ \dot{u}_2 \end{Bmatrix}+\begin{bmatrix} k_1 & 0 \\ 0 & k_2 \end{bmatrix}\begin{Bmatrix} u_1 \\ u_2 \end{Bmatrix}=-\begin{bmatrix} m_1 & 0 \\ 0 & m_2 \end{bmatrix}\begin{Bmatrix} 1 \\ 1 \end{Bmatrix}\ddot{u}_g \quad (4)$$

- for the two corresponding disconnected damped SDOF systems:

$$m_1\ddot{u}_{SDOF1}+(c_{in1}+c_d)\dot{u}_{SDOF1}+k_1u_{SDOF1}=-m_1\ddot{u}_g \quad (5)$$

$$m_2\ddot{u}_{SDOF2}+(c_{in2}+c_d)\dot{u}_{SDOF2}+k_1u_{SDOF2}=-m_2\ddot{u}_g \quad (6)$$

The fundamental dynamic properties of the two disconnected damped SDOF systems are indicated as it follows. $\omega_{1n}=\sqrt{\frac{k_1}{m_1}}$ and $\omega_{2n}=\sqrt{\frac{k_2}{m_2}}$ are the undamped natural frequencies of SDOF systems 1 and 2, respectively; $\xi_{1n}=\frac{c_{in1}+c_d}{2m_1\omega_{1n}}$ and $\xi_{2n}=\frac{c_{in2}+c_d}{2m_2\omega_{2n}}$ are the corresponding damping ratios. The suffix *n* refers to the natural undamped mode of vibration. The periods of vibration corresponding to ω_{1n} and ω_{2n} are denoted as T_{1n} and T_{2n}, respectively.

It is useful to introduce the following dimensionless parameters: frequency ratio $\Omega=\frac{\omega_{1n}}{\omega_{2n}}$, mass ratio $\rho=\frac{m_1}{m_2}$ and normalized damping coefficient $\xi_d=\frac{c_d}{2m_1\omega_{1n}}$. Note that the normalized damping coefficient is coincident with the damping ratio of the damped SDOF system 1 in case of null intrinsic damping coefficient c_{in1}.

The dynamic response of the system is investigated varying the key parameters within the range indicated in Table 1.

Table 1: Ranges of the key parameters considered in the parametric analysis.

	Period T_{1n}	Mass ratio ρ	Frequency ratio Ω	Normalized viscous damping ratio ξ_d
Range	0.5 s; 1.0 s; 1.5 s	0.5; 1.0; 2.0	0.2 - 4.0 (step 0.1)	0.2 - 4.0 (step 0.1)

3.2. Dynamic properties

The dynamic equilibrium equation of the coupled one-storey system with null intrinsic damping coefficients (e.g. c_{in1}=c_{in2}=0) under free vibration reads:

$$\begin{cases} m_1\ddot{u}_1+c_d\left(\dot{u}_1-\dot{u}_2\right)+k_1u_1=0 \\ m_2\ddot{u}_2+c_d\left(\dot{u}_2-\dot{u}_1\right)+k_2u_2=0 \end{cases} \quad (7)$$

According to the theory of complex damping, the characteristic equation of the system can be written as follows:

$$k_1k_2+(k_1+k_2)c_d\lambda+(k_1m_2+k_2m_1)\lambda^2+(m_1+m_2)c_d\lambda^3+m_1m_2\lambda^4=0 \quad (8)$$

It is convenient to express the characteristic equation in terms of dimensionless coefficients Ω, ρ, and ξ_d:

$$\frac{\omega_{1n}^{\ 4}}{\Omega^2}+2(1+\frac{\Omega^2\rho}{\Omega^2})\xi_d\omega_{1n}^{\ 3}\lambda+\left(\frac{1+\Omega^2}{\Omega^2}\right)\omega_{1n}^{\ 2}\lambda^2+2(1+\rho)\xi_d\omega_{1n}\lambda^3+\lambda^4=0 \tag{9}$$

Eq. 9 is a fourth order algebraic equation and, in general, has four complex roots (k = 1, …, 4) of the following general form:

$$\lambda_k=-\xi_k\omega_k+i\sqrt{1-\xi_k^{\ 2}}\omega_k \tag{10}$$

where $\xi_k=\dfrac{\mathrm{Re}(\lambda_k)}{\omega_k}$ and $\omega_k=|\lambda_k|=\sqrt{\mathrm{Re}(\lambda_k)^2+\mathrm{Im}(\lambda_k)^2}$ are called the k-th damping ratio and undamped frequency, respectively. For an underdamped system, the four eigenvalues are complex conjugates pairs. The imaginary part of the k-th complex frequency, $\omega_{dk}=\mathrm{Im}(\lambda_k)=\sqrt{1-\xi_k^{\ 2}}\omega_k$, is the damped frequency. In general, the k-th undamped frequency ω_k may differ from its corresponding natural undamped frequency ω_{kn} due to the non-proportionality of the damping matrix.

The graphs of Figures 4 and 5 provide the trends of the damping ratios ξ_k and undamped frequencies ω_k vs ξ_d for the general case of $\Omega \neq 1.0$ and for the specific case of $\Omega = 1.0$, respectively. For comparison purposes, also the damping ratios and the undamped natural frequencies of the corresponding damped SDOF systems are included in the graphs.

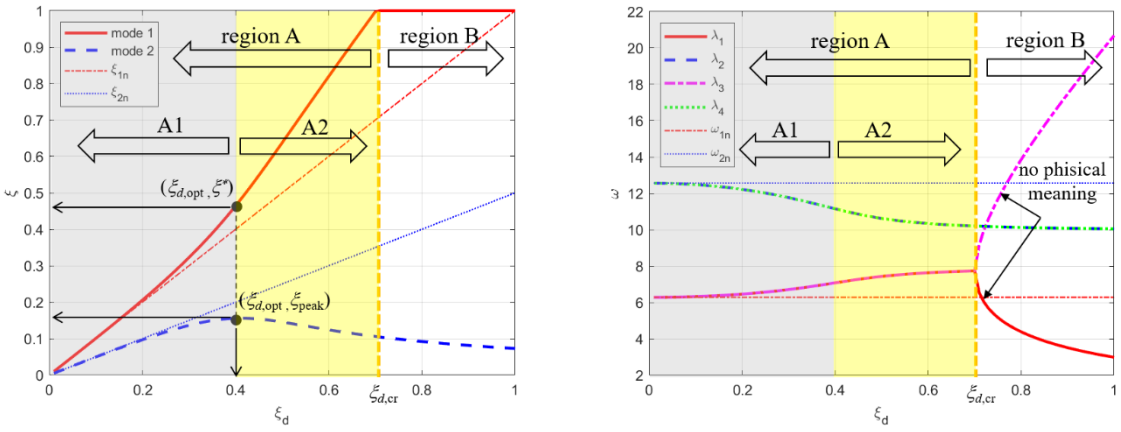

(a) (b)

Figure 4: Damping ratios (a) and undamped frequencies (b) for Ω = 0.5 and ρ = 1.0.

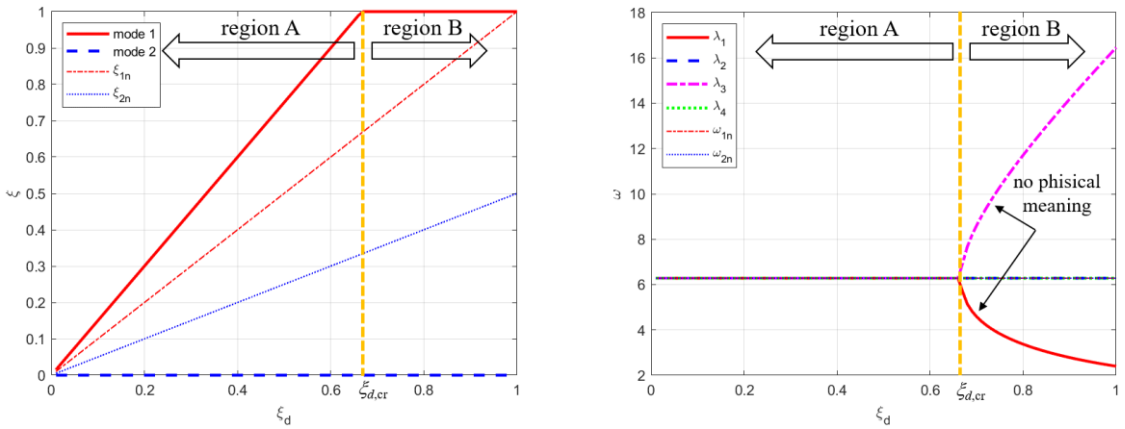

(a) (b)

Figure 5: Damping ratios (a) and undamped frequencies (b) for $\Omega = 1.0$ and $\rho = 0.5$.

The following observations can be made:

- For the general case of $\Omega \neq 1.0$, the four roots represent two complex modes with two different undamped frequencies up to the critical normalized damping coefficient $\xi_{d,cr}$ that represents the limit of two regions of behaviour: region A characterized by $\xi_d \leq \xi_{d,cr}$ and region B characterized by $\xi_d > \xi_{d,cr}$.

  In region B one mode is overdamped, therefore only one frequency has a physical meaning. The damping ratio of the remaining mode decreases with increasing values of ξ_d.

  In region A both modes are underdamped, and their frequencies tend to get closer and closer with increasing values of ξ_d. One damping ratio increases for increasing values of ξ_d up to a unit value reached at $\xi_d = \xi_{d,cr}$, while the other one first achieves a peak value ξ_{peak} for $\xi_d = \xi_{d,opt}$ and then progressively decreases for ξ_d values larger than $\xi_{d,opt}$. The damping coefficient of the viscous damper that corresponds to $\xi_{d,opt}$ can be interpreted as an optimum damping coefficient, since it leads to the peak value of one damping ratio. The value of the other damping ratio at $\xi_d = \xi_{d,opt}$ is indicated as ξ^*. In general, the extent of region A depends on the key parameters of the system. Within region A, two further sub-regions can be distinguished: region A1 characterized by $\xi_d \leq \xi_{d,opt}$ and region A2 characterized by $\xi_{d,opt} < \xi_d \leq \xi_{d,cr}$. In region A1 the two damping ratios are very close to the damping ratios of the two corresponding undamped SDOF systems. This indicates a low coupling of modes. In other words, almost the entire damping coefficient is effective in providing energy dissipation. On the contrary, within region A2, the trends of both the two damping ratios and undamped frequencies diverge significantly from those of the corresponding damped SDOF systems, thus indicating a significant coupling between modes. Therefore, in this region, only a small fraction of the damping coefficient is effective in providing energy dissipation, while the remaining fraction is responsible for

energy transfer between modes. The specific values of $\xi_{d,cr}$, $\xi_{d,opt}$, ξ_{peak} and ξ^* govern the dynamic behaviour of the coupled system and are highly dependent on the key dynamic parameters, as it will be clarified in sections 3.3 and 4.

- In the specific case of Ω = 1.0, the two complex modes have an equal and constant (i.e. not influenced by ξ_d) undamped frequency within the entire range of ξ_d. In region B, only one frequency has a physical meaning. In region A, one damping ratio linearly increases up to a unit value for increasing values of ξ_d up to $\xi_{d,cr}$, with a slope larger than the ones of the damping ratios of the two corresponding undamped SDOF systems. On the contrary, the other damping ratio remains identically null for all values of ξ_d. This means that one mode is a damped mode, whilst the other is an undamped mode independently from the value of ξ_d. The undamped mode corresponds to an in-phase motion of the two buildings leading therefore to a null relative displacement (and velocity) $|u_2 - u_1|$ and to a null damping force, since the whole system made of the two coupled structures oscillates in unison. The damped mode corresponds to an out-of-phase motion of the two buildings.

3.3. Influence of the key system parameters on the dynamic properties of the coupled system

This paragraph discusses the influence of the key system parameters Ω and ρ on the dynamic properties of the coupled system, with particular focus on the damping ratios $\xi_{d,cr}$, $\xi_{d,opt}$, ξ_{peak} and ξ^* identified in the previous section. For this aim, Figure 6 shows the trends of the above-mentioned damping ratios vs. ξ_d for eight different Ω values and for constant ρ=1.0. For Ω=1.0, the values of ξ_{1n} and ξ_{2n} are equal to each other since the two undamped SDOF systems have the same natural period and the same mass. For Ω values larger than 1.0, the order of modes is switched with respect to the case of Ω values smaller than 1.0.

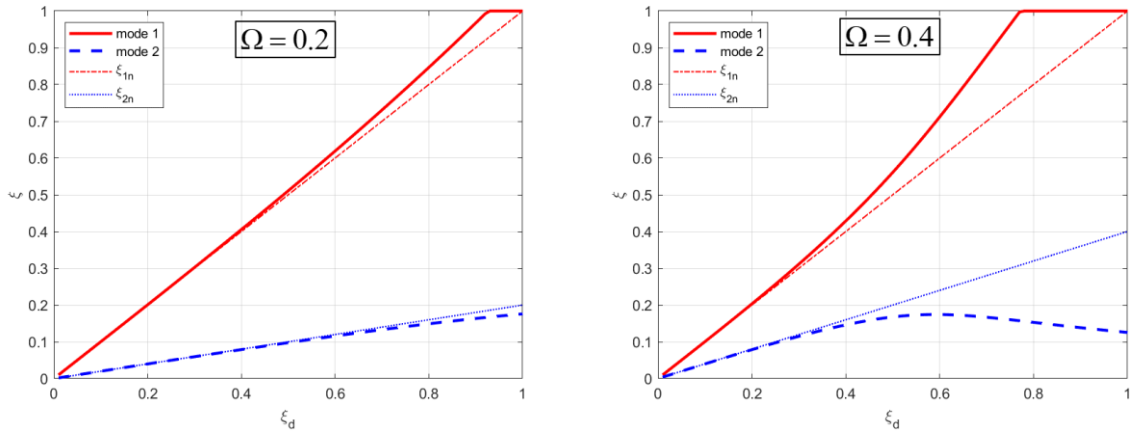

(a) (b)

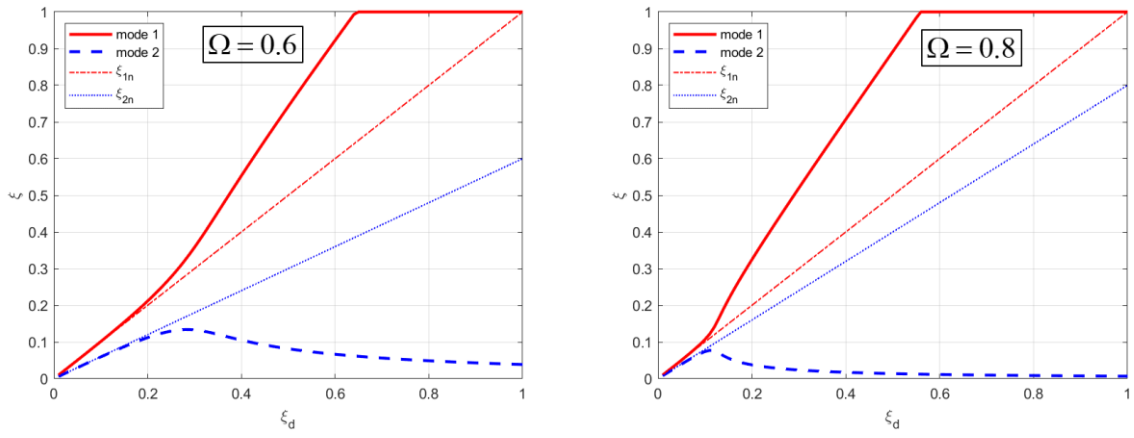

(c)

(d)

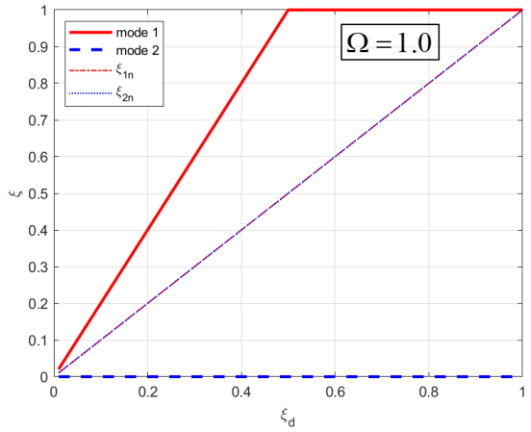

(e)

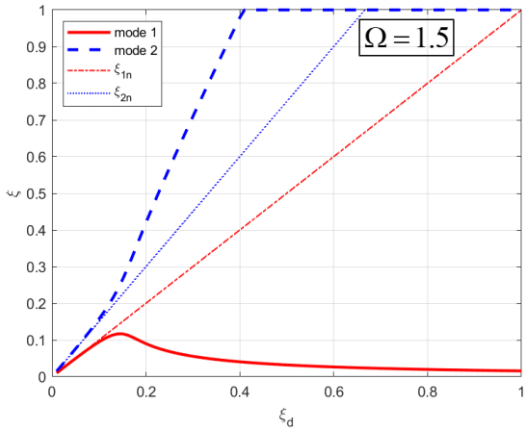

(f)

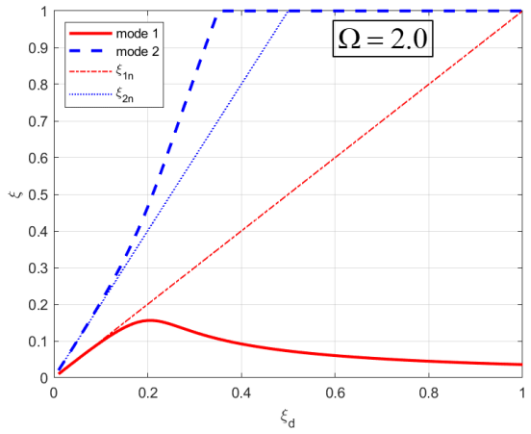

(g)

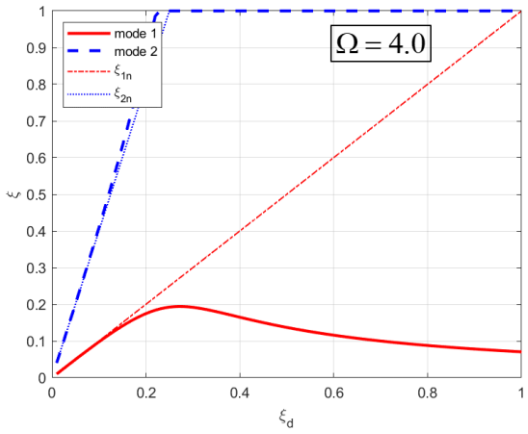

(h)

Figure 6: Damping ratios for constant mass ratio (ρ=1.0) and: (a) Ω=0.2; (b) Ω=0.4; (c) Ω=0.6; (d) Ω=0.8; (e) Ω=1.0; (f) Ω=1.5; (g) Ω=2.0; (h) Ω=4.0.

For small values of Ω (for instance, refer to Figure 6a corresponding to Ω=0.2), the width of region A is large since the critical condition is achieved for ξ_d values larger than 0.8 ($\xi_{d,cr} \geq 0.8$); the value ξ_{peak} is reached at a $\xi_{d,opt}$ larger than 1.0; ξ^* is equal to 1.0. In these cases, the system is weakly coupled within the full range of ξ_d<1.0. For increasing values of Ω (0.4< Ω< 0.8), the width of region A progressively decreases and the values of $\xi_{d,opt}$ result to be very sensitive to Ω. The corresponding ξ_{peak} remain limited around 0.2. For instance, when considering the case of Ω =0.6 (Figure 6c), a value of ξ_{peak} around 0.15 is reached for $\xi_{d,opt}$ around 0.3 with a ξ^* value also around 0.3. The divergence of the damping ratios from those of the corresponding damped SDOF systems indicate the raising of the coupling effects, causing the progressively reduction of one damping ratio. For 0.6< Ω< 0.8, this condition occurs at ξ_d values around 0.2. In these cases, the energy transfer effect is predominant with respect to the energy dissipation effect. In other words, from a physical point of view, for the case of buildings with comparable floor masses, the presence of a support structure with stiffness of the same order of magnitude of that of the reference structure limits the full exploitation of the total damping coefficient c_d (or its normalized version ξ_d) theoretically available for energy dissipation.

Figures 7 and 8 provide curves and surfaces of $\xi_{d,cr}$, $\xi_{d,opt}$, ξ_{peak} and ξ^*, respectively. First of all, it can be noted that all damping ratios appear to be very sensitive to both Ω and ρ parameters. Note that the values of $\xi_{d,opt}$, ξ_{peak} and ξ^* are not defined for Ω=1.0.

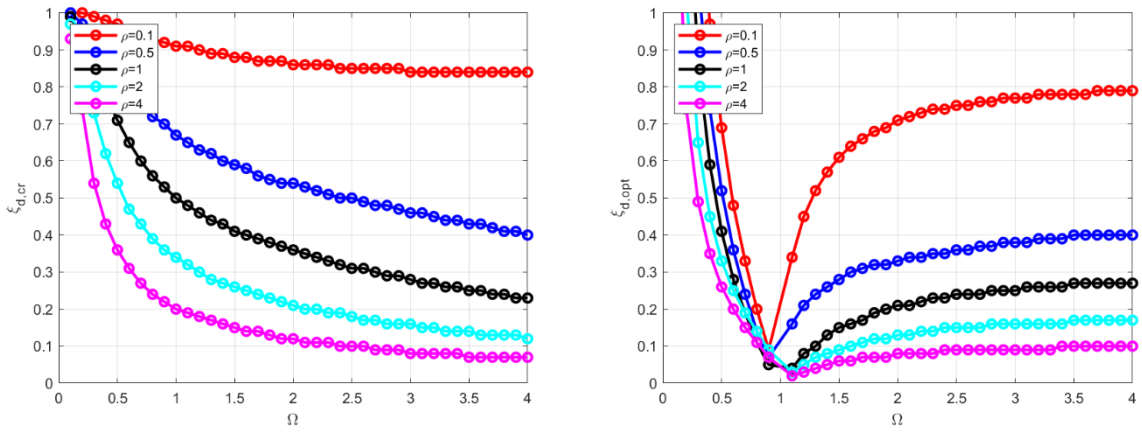

(a) (b)

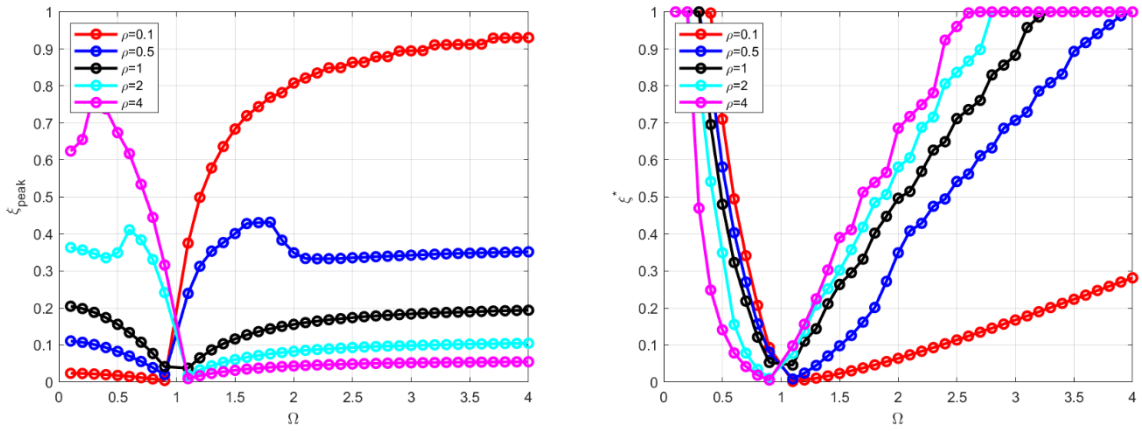

(c) (d)

Figure 7:(a) $\xi_{d,cr}$ vs Ω ; (b) $\xi_{d,opt}$ vs Ω ; (c) ξ_{peak} vs Ω ; (d) ξ^* vs Ω , for different ρ values.

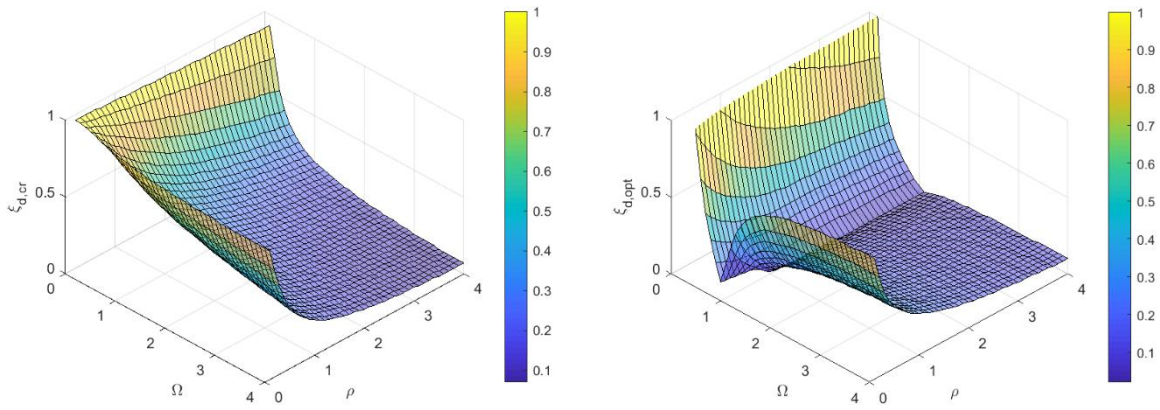

(a) (b)

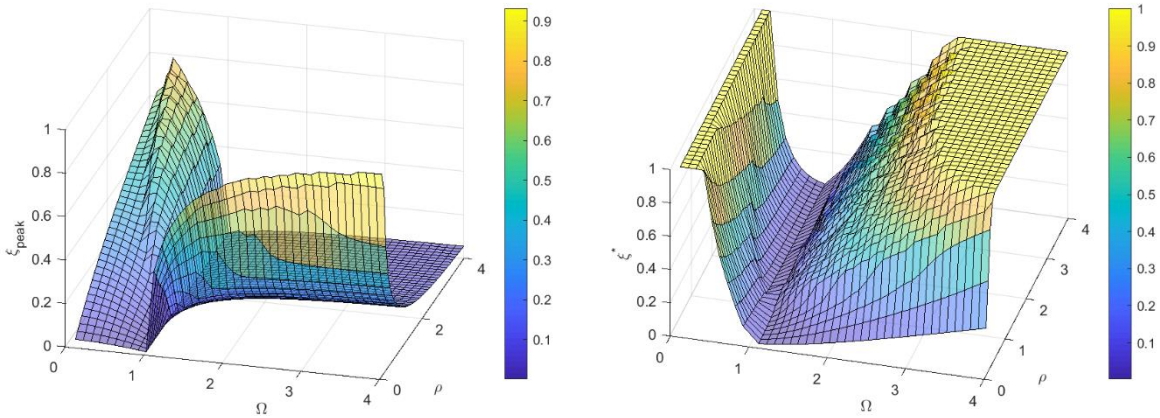

(c) (d)

Figure 8:(a) $\xi_{d,cr}$ vs Ω and ρ ; (b) $\xi_{d,opt}$ vs Ω and ρ ; (c) ξ_p vs Ω and ρ ; (d) ξ^* vs Ω and ρ.

The values of $\xi_{d,cr}$ progressively decrease for increasing values of both Ω and ρ. The decrease with Ω is very fast for Ω values within the range of 0.0 and 1.0. Then the curves become flatter.

The trends of both $\xi_{d,opt}$, ξ_{peak} and ξ^* vary significantly when Ω values get smaller or larger than 1.0.

$\xi_{d,opt}$ values first rapidly decrease for Ω values between 0.0 and 1.0, and are not much influenced by ρ. Then, for Ω values larger than 1.0, they progressively increase and become very sensitive to ρ values. In particular, for small values of ρ, large values of $\xi_{d,opt}$ (up to 0.8) are achieved. For larger ρ values, the increase of $\xi_{d,opt}$ is less significant.

Values of ξ_{peak} also first decrease with Ω values going from 0.0 to 1.0. The rate of decrease is very sensitive to ρ. For large ρ values, ξ_{peak} values tend to be larger. Then, for Ω values larger than 1.0, ξ_{peak} values tend to increase with increasing values of Ω with trends that are qualitatively similar to those of $\xi_{d,opt}$.

Values of ξ^* are equal to 1.0 for small Ω values, while they rapidly decrease as Ω values approach 1.0. Then, for Ω values larger than 1.0, ξ^* values tend to increase again, almost linearly with slopes depending on ρ. The larger ρ, the steeper the slope.

To sum up, the optimal systems are identified in terms of Ω and ρ, as those able to maximize the damping parameters ξ_{peak} and ξ^*. Then, for the identified optimal systems, the parameter $\xi_{d,opt}$ may guide to select the optimal damping coefficient $c_{d,opt} = 2\xi_{d,opt} m_1 \omega_{1n}$. Nevertheless, the system effectiveness also depends on the characteristics of the dynamic input. The influence of the main parameters on the dynamic response of the system will be analysed in the next sections, considering both harmonic (section 3.4) and earthquake (section 3.5) ground excitations.

3.4. Frequency response curves and surfaces

Frequency response curves are determined considering an harmonic displacement of peak amplitude D_g and frequency ω_g, $u_g(t) = D_g e^{i\omega_g t}$, applied at the ground level:

$$\begin{cases} m_1\ddot{u}_1 + c_d\left(\dot{u}_1 - \dot{u}_2\right) + k_1 u_1 = -m_1\ddot{u}_g \\ m_2\ddot{u}_2 + c_d\left(\dot{u}_2 - \dot{u}_1\right) + k_2 u_2 = -m_2\ddot{u}_g \end{cases} \tag{11}$$

Assuming harmonic stationary solutions of the type $u_1(t) = D_1 e^{i\omega_g t}$ and $u_2(t) = D_2 e^{i\omega_g t}$, and introducing the dimensionless frequency parameters $\beta = \omega_g / \omega_{1n}$ and $\beta_2 = \omega_g / \omega_{2n} = \beta\Omega$, it is then possible to obtain the following analytical expressions of the complex amplitudes D_1 and D_2 of relative displacements u_1 and u_2:

$$D_1 = D_g\beta^2\left[\frac{-1+\Omega^2\beta\left(\beta-2i\xi_d\left(1+\rho\right)\right)}{1-\left(1+\Omega^2\right)\beta^2+\Omega^2\beta^4-2i\Omega^2\beta^3\xi_d\left(1+\rho\right)+2i\beta\left(\xi_d+\Omega^2\xi_d\rho\right)}\right]$$

$$D_2 = D_g\left(\Omega\beta\right)^2\left[\frac{-1+\beta^2-2i\beta\xi_d\left(1+\rho\right)}{1-\left(1+\Omega^2\right)\beta^2+\Omega^2\beta^4-2i\Omega^2\beta^3\xi_d\left(1+\rho\right)+2i\beta\left(\xi_d+\Omega^2\xi_d\rho\right)}\right] \quad (12)$$

It is then possible to evaluate the analytical expressions of $|D_1|/\left(D_g\beta^2\right)|$ and $|D_2|/\left(D_g\left(\beta\Omega\right)^2\right)$ which provide the moduli of the complex amplitudes as normalized with respect to the static responses of Building 1 and Building 2, respectively, namely the dynamic amplification factors of the two degrees of freedom. Analytical expressions of the displacement dynamic amplification factors were determined by Bhaskararao and Jangid 2007 [9]. In the special case of Ω=1.0, the expressions of the complex amplitudes D_1 and D_2 reduce to the same real value:

$$D_1 = D_2 = \frac{D_g\beta^2}{\beta^2-1} \quad (13)$$

and the amplification factors become equal to $|D_1|/\left(D_g\beta^2\right)=|D_2|/\left(D_g\left(\beta\Omega\right)^2\right)=1/\left(\beta^2-1\right)$. Note that the expression $1/\left(\beta^2-1\right)$ represents the dynamic amplification of an undamped SDOF system (Chopra 2001 [19]).

The graphs displayed in Figures 9 and 10 provide frequency response curves (vs β) and surfaces (vs β and ξ_d) of the dynamic amplification factors related to D_1 and D_2 (i.e. $|D_1|/\left(D_g\beta^2\right)|$ and $|D_2|/\left(D_g\left(\beta\Omega\right)^2\right)$), respectively. In detail, the frequency response curves shown in Figure 9 are represented for selected Ω (0.4 and 2.0) and ρ (0.2, 1.0, 1.5 and 2.0) values and for a fixed ξ_d value (0.15). For comparison purposes, also the frequency response curve of the damped SDOF system with natural undamped frequency ω_{1n} and damping ratio ξ=0.15 is provided.

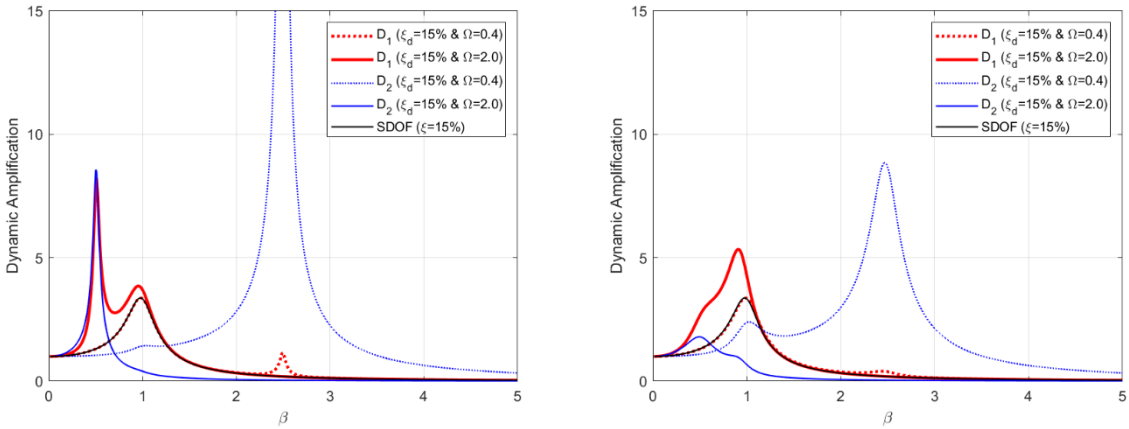

(a) (b)

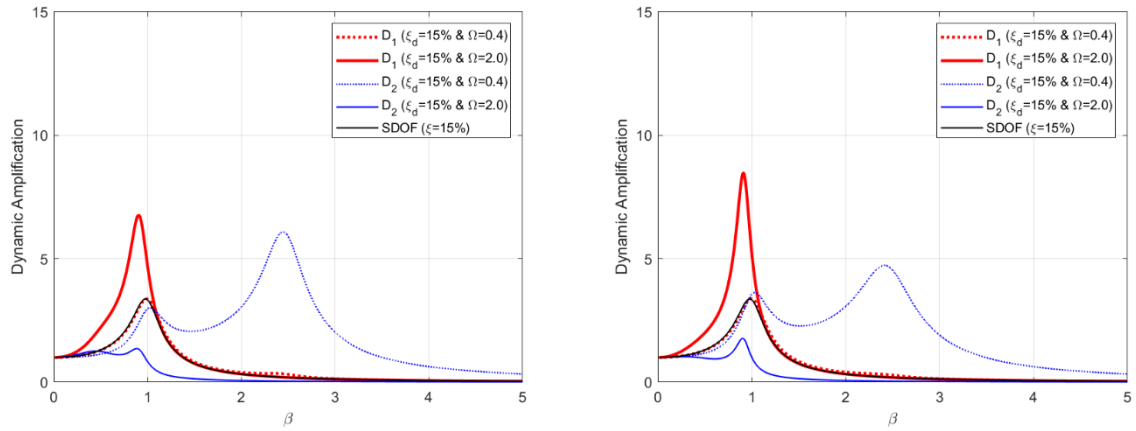

(c) (d)

Figure 9: Frequency response curves for: (a) $\rho = 0.2$; (b) $\rho = 1.0$; (c) $\rho = 1.5$; (d) $\rho = 2.0$.

As well known, the curve of the SDOF system is characterized by a single peak around $\beta = 1.0$ with amplitude equal to $1/(2\xi)$ (that, in this specific case, is equal to 3.33).

The frequency response curves of the coupled system have, instead, two peaks at frequencies equal to the damped frequencies ω_{d1} and ω_{d2}. Note that the peak around $\beta = 1.0$ corresponds to the amplification at the first damped frequency ω_{d1}, while the other peak (around β =2.5 for Ω =0.4 and β =0.5 for Ω =2.0) corresponds to the amplification at the other damped frequency ω_{d2}. For Ω=0.4, the peak amplification of D_1 around $\beta = 1.0$ is close to that of the corresponding damped SDOF system, independently from ρ. On the contrary, the peak amplification of D_2 around $\beta = 2.5$ is significantly influenced by ρ: for small ρ values the amplification is very large (>15), while for increasing ρ values, the amplification progressively decreases. For Ω=2.0, the peak amplification of D_1 around $\beta = 1.0$ is larger than that of the corresponding damped SDOF system and tends to increase with increasing ρ values. On the contrary, the peak amplification of D_2 around $\beta = 0.5$ strongly reduces with increasing ρ values.

The frequency response surfaces represented in Figure 10 allow to appreciate the influence of ξ_d on the dynamic amplification factors related to D_1 and D_2.

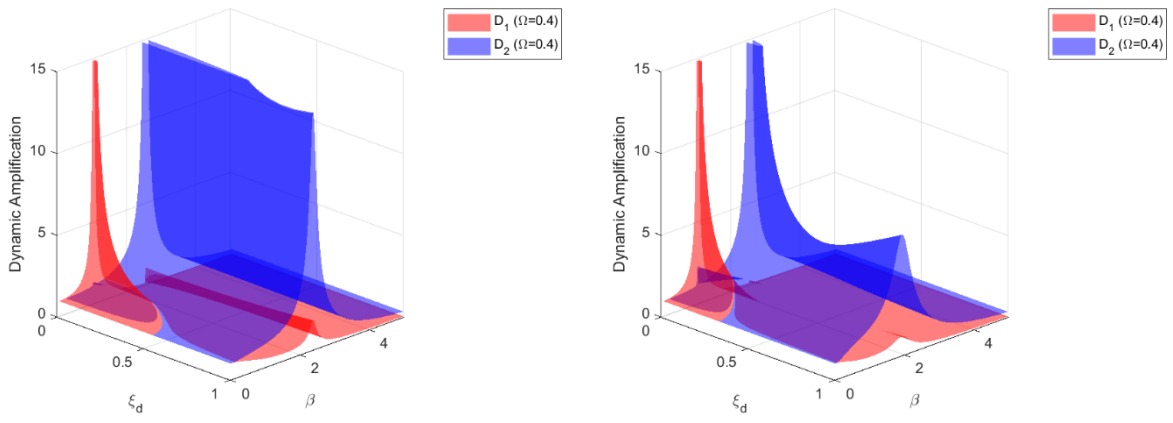

(a) (b)

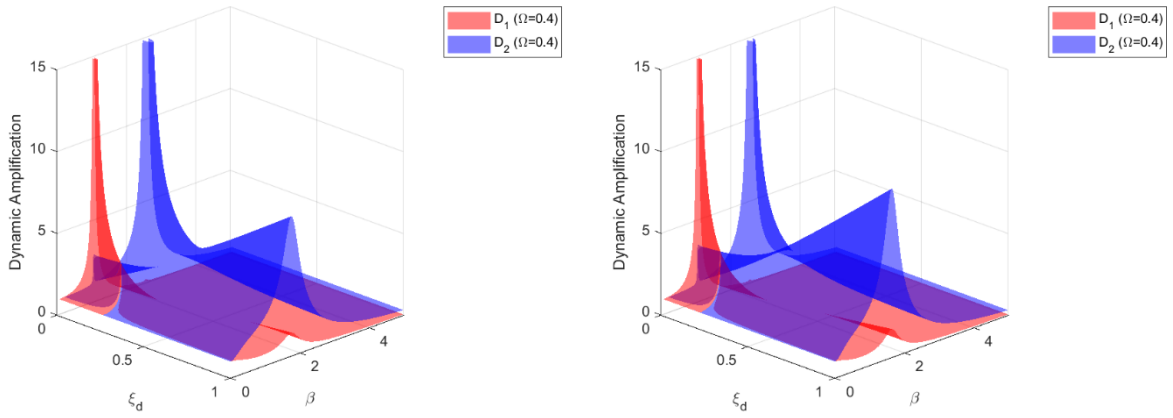

(c) (d)

Figure 10: Frequency response surfaces for Ω=0.4 and: (a) ρ=0.2; (b) ρ=1.0; (c) ρ=1.5; (d) ρ=2.0.

As long as ξ_d remains below a certain value, the peak amplifications rapidly decrease with increasing ξ_d values. On the contrary, for larger ξ_d values the peak amplifications of the coupled system tend to increase with increasing ξ_d values.

3.5. Displacement reduction factors under earthquake excitation

The response of the coupled system under earthquake ground motion is investigated with the purpose of evaluating the trends of the damping reduction factors of the peak displacements with respect to ξ_d and the key parameters Ω, ρ and T_{1n} (i.e. the period of vibration of the reference structure). The following damping reduction factors are introduced:

$$\eta_1(\xi_d) = \frac{u_{1,\max,\xi_d}}{u_{1,\max,\xi_d=0}} \tag{14}$$

$$\eta_2(\xi_d) = \frac{u_{2,\max,\xi_d}}{u_{2,\max,\xi_d=0}} \tag{15}$$

$$\eta_{SDOF1}(\xi_d) = \frac{u_{SDOF1,\max,\xi_d}}{u_{SDOF1,\max,\xi_d=0}} \tag{16}$$

$$\eta_{SDOF2}(\xi_d) = \frac{u_{SDOF2,\max,\xi_d}}{u_{SDOF2,\max,\xi_d=0}} \tag{17}$$

where $u_{1,\max,\xi_d}$, $u_{2,\max,\xi_d}$, $u_{SDOF1,\max,\xi_d}$ and $u_{SDOF2,\max,\xi_d}$ are the peak displacements of degrees of freedom u_1, u_2, u_{SDOF1}, and u_{SDOF2}, respectively. Similarly, $u_{1,\max,\xi_d=0}$, $u_{2,\max,\xi_d=0}$, $u_{SDOF1,\max,\xi_d=0}$ and $u_{SDOF2,\max,\xi_d=0}$ are the peak displacements for the specific value of ξ_d = 0. In all cases, inherent damping coefficients c_{1h} and c_{2h} leading to inherent damping ratios equal to 5% are considered in addition to the damping ratio provided by the added viscous damper. It can be noted that $u_{1,\max,\xi_d=0} = u_{SDOF1,\max,\xi_d=0}$ and $u_{2,\max,\xi_d=0} = u_{SDOF2,\max,\xi_d=0}$.

Figures 11 and 12 provide curves and surfaces of the average values (over the 10 accelerograms described in section 2.2) of the displacement reduction factors, respectively. Figures 11a and b display the trends of the reduction factors η_1 and η_2 as a function of ξ_d for selected Ω values (0.2, 0.5, 1.5, 2 and 4) and for ρ = 1.0 and T_{1n} = 0.5s, together with η_{SDOF1} and η_{SDOF2}, respectively. For comparison purposes, also the well-known relationship by Bommer et al. 2000 [30] is represented in the graphs of Figure 11.

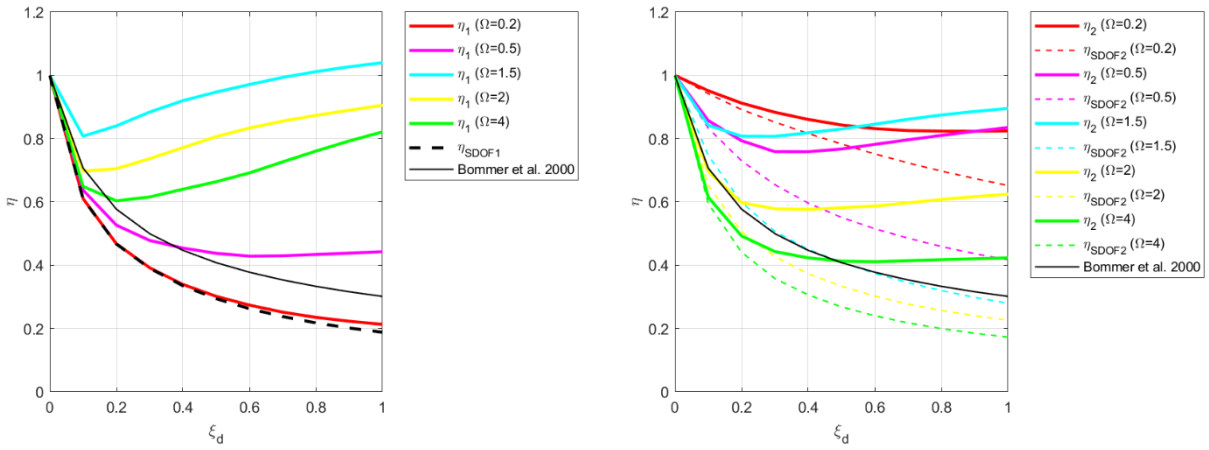

(a) (b)

Figure 11: Displacement reduction factors for ρ = 1.0 and T_{1n} = 0.5s: (a) η_1; (b) η_2.

As far as η_1 is concerned, for small Ω values (refer, for instance, to the curve related to Ω=0.2 corresponding to the case with SDOF system 2 much stiffer - 25 times - than SDOF system 1) the trends of η_1 follows the one of the corresponding damped SDOF system. On the contrary, systems with Ω values around 0.5 (SDOF system 2 is four times stiffer than SDOF system 1) show a reduction factor η_1 that first decreases up to a certain value of ξ_d=ξ_{dp} (around 0.2) and then remains almost constant for $\xi_d \geq \xi_{dp}$. At ξ_d=ξ_{dp} reduction factor values are around 0.4-0.5 depending on the value of T_{1n}. Systems with Ω values larger than 0.5 (the two SDOF systems have a similar stiffness) exhibit very limited reductions of the peak displacement (e.g. large values of η_1). For the cases represented in Figure 11a, the maximum reductions at ξ_{dp} correspond to reduction factor values around 0.7-0.8. For values of ξ_d>ξ_{dp}, the reduction factors increase and may achieve values even larger than 1.0 (detrimental effects).

As far as η_2 is concerned, the smallest reduction factor values (i.e. the largest reductions in the peak displacement response) are observed for large values of Ω (refer, for instance, to the curve related to Ω = 4 corresponding to the case with SDOF system 1 much stiffer - 16 times - than SDOF system 2). For values of Ω <1.0, the η_2 values are limited to 0.8 (e.g. 20% reduction) at ξ_{dp}, while, for larger ξ_d values, they slightly increase.

Figures 12a, c and e display surfaces of η_1 as function of ξ_d and Ω for selected ρ and T_{1n} values, while Figures 12 b, d and f display surfaces of η_2. Both ρ and T_{1n} parameters have a slight influence on the trends of η_1.

The minimum values of η_1 and η_2 (namely $\eta_{1\min}$ and $\eta_{2\min}$) and corresponding ξ_d values (namely ξ_{d1}^* and ξ_{d2}^*) have been computed to evaluate the influence of the main key parameters Ω, ρ and T_{1n}. Figures 13 and 14 display the curves of $\eta_{1\min}$ and $\eta_{2\min}$ and of ξ_{d1}^* and ξ_{d2}^* as functions of Ω, for selected values of ρ and

T_{1n}, respectively. Figure 15 displays the surfaces of $\eta_{1\min}$ and $\eta_{2\min}$ as functions of Ω and ρ, for selected values of T_{1n}.

It can be noted that both $\eta_{1\min}$ and $\eta_{2\min}$ are primarily influenced by Ω, while their dependency upon both ρ and T_{1n} is less significant. In particular, $\eta_{1\min}$ first increases (almost linearly) for values of Ω up to 1.0. Then, for $\Omega \geq 1.0$, a decreasing trend (almost hyperbolic) up to a value of around 0.6-0.7 at Ω=4.0 is observed. Values of $\eta_{2\min}$ oscillate between 0.7-1.0 for $\Omega \leq 1.0$. Then, for $\Omega \geq 1.0$, a decreasing trend (almost hyperbolic) up to a value of around 0.2-0.5 at Ω=4.0 is observed. The trends of ξ_{d1}^{*} are similar to those of $\xi_{d,opt}$ (Figure 7b), since, due to the coupling effects, they exhibit a quite sudden drop to the 0.1 value for increasing values of Ω up to 1.0. For $\Omega \geq 1.0$, ξ_{d1}^{*} values tend to remain almost constant around 0.2-0.3. Values of ξ_{d2}^{*} tend to first increase for $\Omega \leq 1.0$ (the increase is less significant for small ρ values), then a drop is evidenced for $\Omega \geq 1.0$.

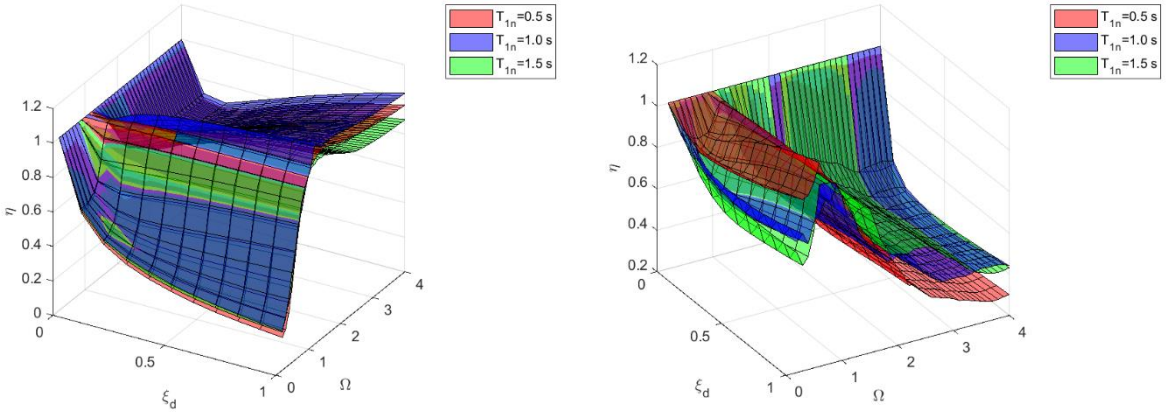

(a) (b)

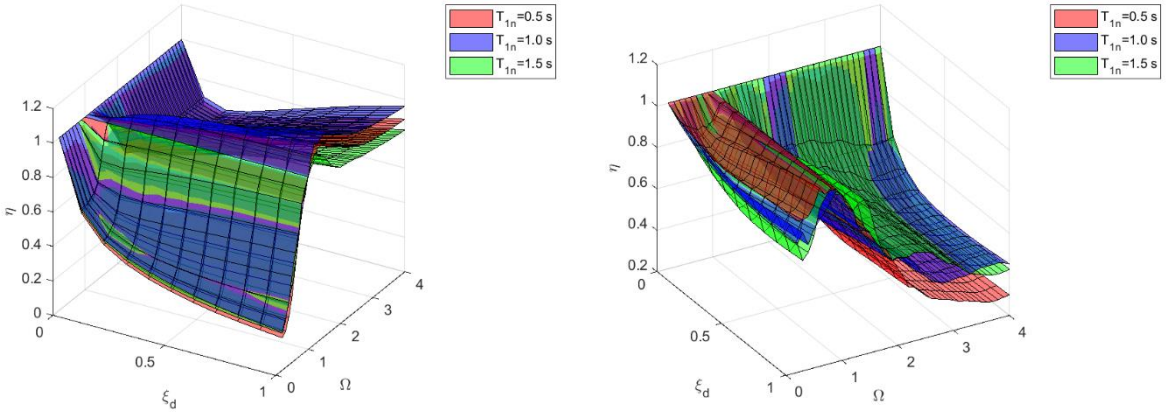

(c) (d)

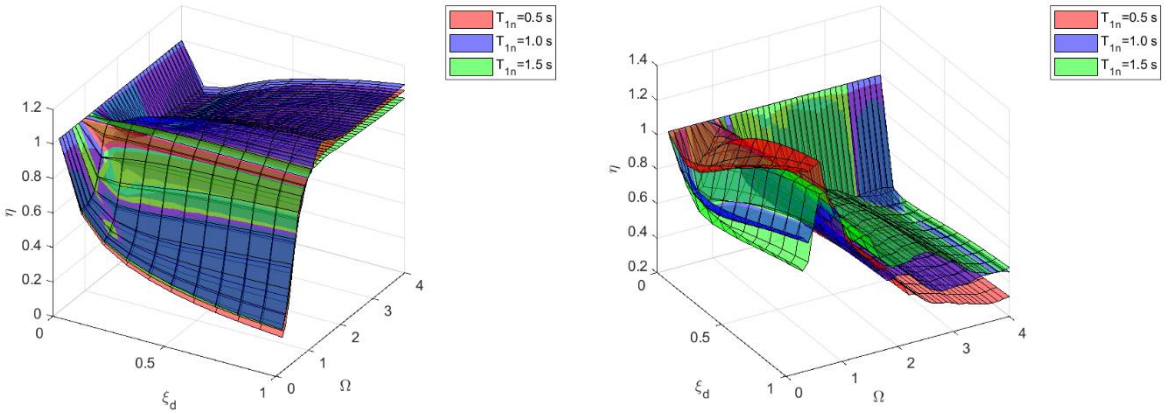

(e) (f)

Figure 12: Displacement reduction factors: (a) η_1 for $\rho = 1.0$; (b) η_2 for $\rho = 1.0$;(c) η_1 for $\rho = 0.5$; (d) η_2 for $\rho = 0.5$; (e) η_1 for $\rho = 2.0$;(f) η_2 for $\rho = 2.0$.

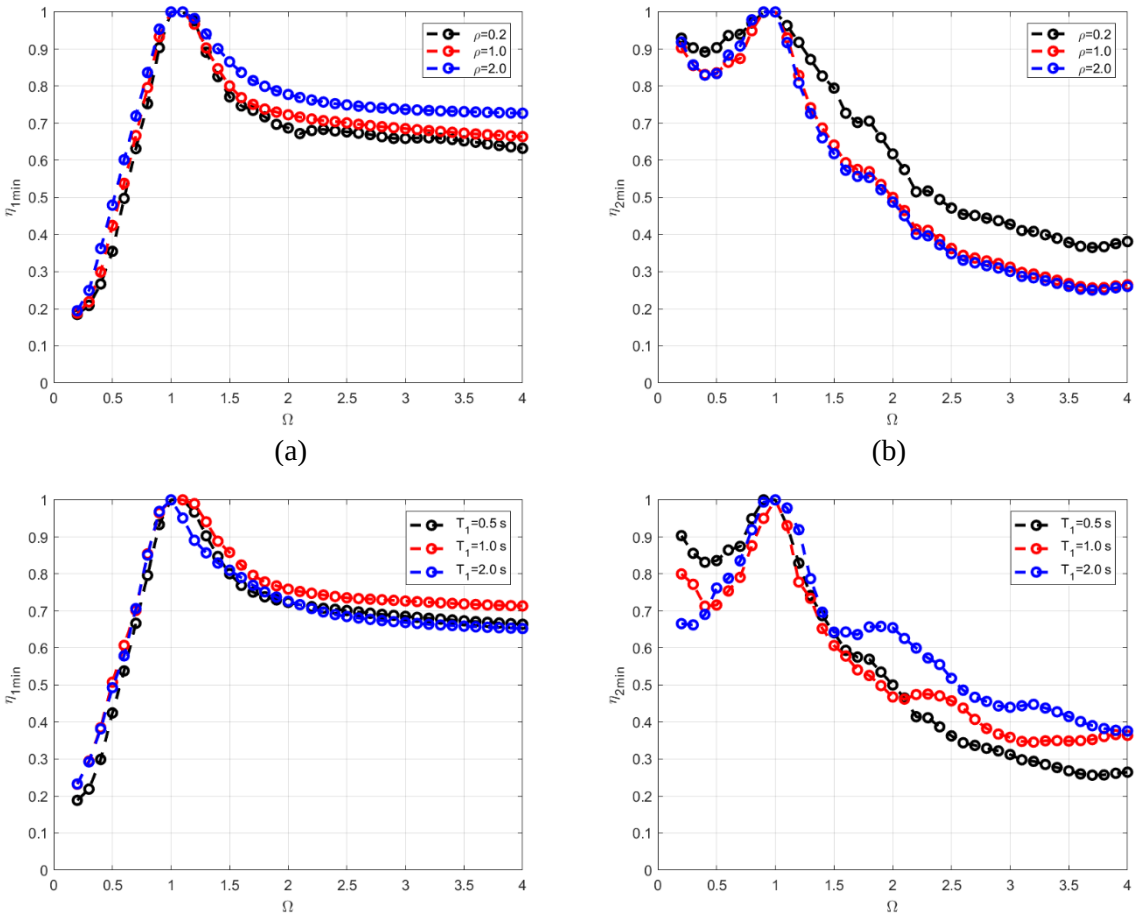

(a) (b)

(c) (d)

Figure 13: Minimum values of the damping reduction factors: (a) η_1 for $T_{1n} = 0.5$ s; (b) η_2 for $T_{1n} = 0.5$ s ; (c) η_1 for $\rho = 1.0$; (d) η_2 for $\rho = 1.0$.

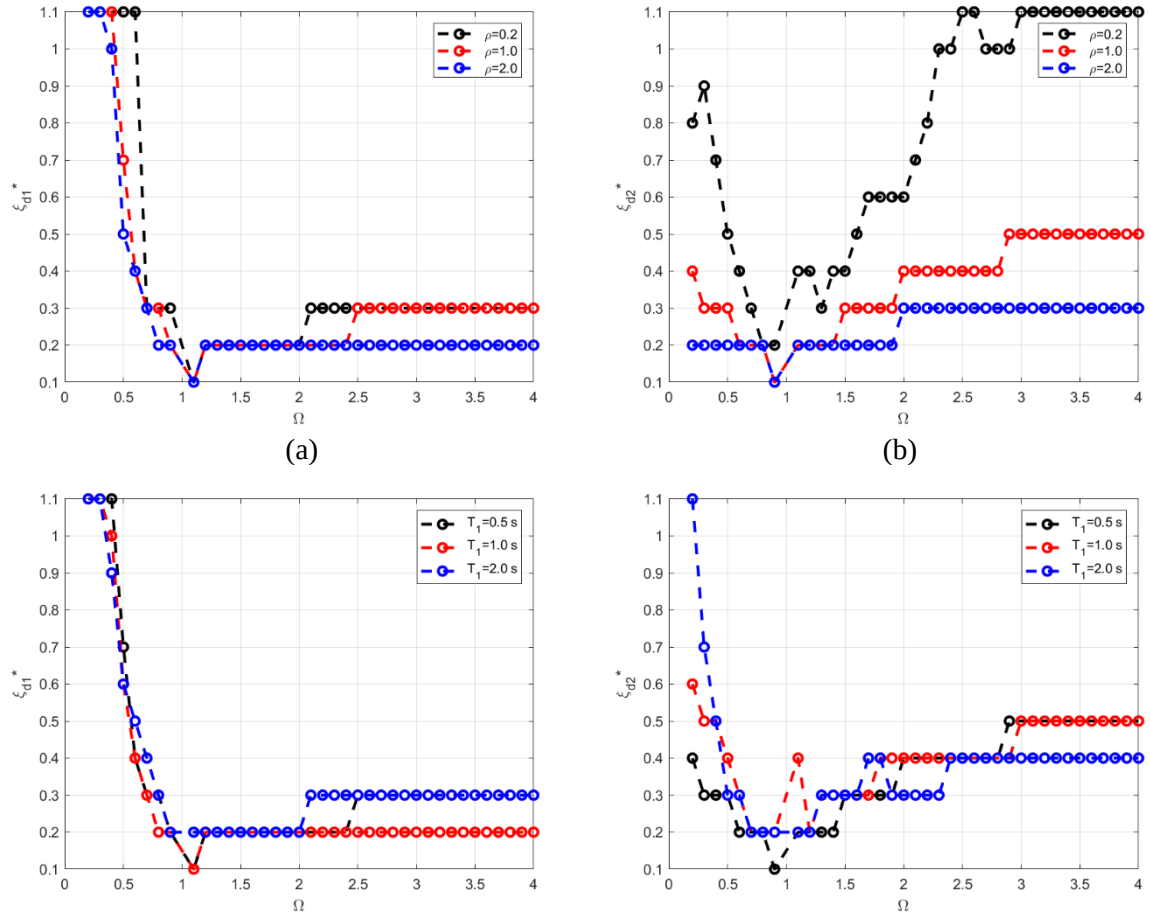

Figure 14: Values of ξ_d corresponding to minimum damping reduction factors: (a) $\xi_{d1}{}^*$ for T_{1n} = 0.5 s; (b) $\xi_{d2}{}^*$ for T_{1n} = 0.5 s; (c) $\xi_{d1}{}^*$ for ρ = 1.0; (d) $\xi_{d2}{}^*$ for ρ = 1.0.

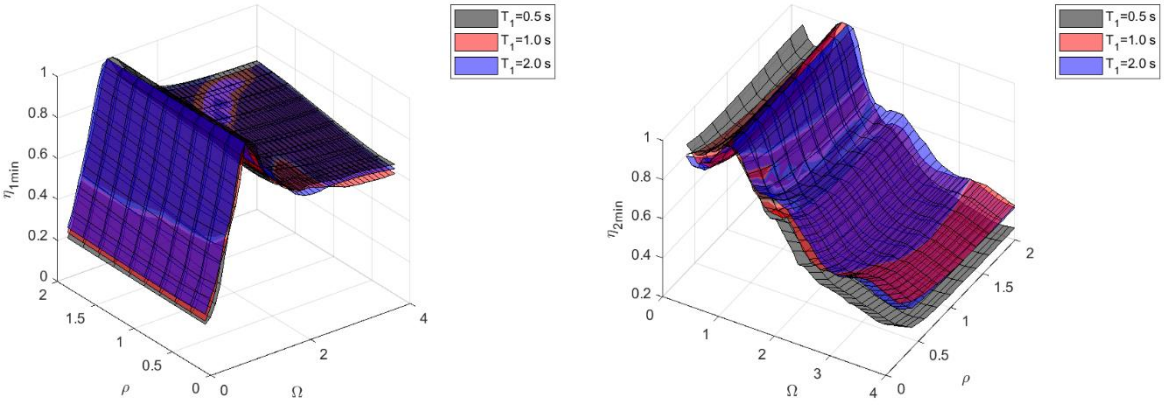

Figure 15: Minimum values of the damping reduction factors: (a) $\eta_{1\min}$; (b) $\eta_{2\min}$.

4. Uniform multi-storey systems

4.1. Considered systems and governing parameters

The present section investigates the seismic behaviour of an N-storey coupled system connected through equal linear viscous dampers (damping coefficients all equal to c_d) placed at all floors. Each building is modelled as a uniform shear-type frame with constant floor mass (equal to m_1 for Building 1 and m_2 for Building 2) and constant lateral stiffness (equal to k_1 for Building 1 and k_2 for Building 2) at all storeys. In such a case, the NxN mass and stiffness matrices of the two individual buildings specialize as follows:

$$\mathbf{M}_1 = \begin{bmatrix} m_1 & & & & \\ & \ldots & & & \\ & & m_1 & & \\ & & & \ldots & \\ & & & & m_1 \end{bmatrix} \tag{18}$$

$$\mathbf{M}_2 = \begin{bmatrix} m_2 & & & & \\ & \ldots & & & \\ & & m_2 & & \\ & & & \ldots & \\ & & & & m_2 \end{bmatrix} \tag{19}$$

$$\mathbf{K}_1 = \begin{bmatrix} 2k_1 & -k_1 & & & \\ -k_1 & \ldots & -k_1 & & \\ & -k_1 & 2k_1 & & \\ & & & \ldots & -k_1 \\ & & & -k_1 & k_1 \end{bmatrix} \tag{20}$$

$$\mathbf{K}_2 = \begin{bmatrix} 2k_2 & -k_2 & & & \\ -k_2 & \ldots & -k_2 & & \\ & -k_2 & 2k_2 & & \\ & & & \ldots & -k_2 \\ & & & -k_2 & k_2 \end{bmatrix} \tag{21}$$

The inherent damping matrix of each building is assumed to be proportional to the mass matrix, that is: $\mathbf{C}_{I1} = a_1\mathbf{M}_1$ and $\mathbf{C}_{I2} = a_2\mathbf{M}_2$, with coefficients a_1 and a_2 selected to obtain a value of the first damping ratio equal to 5% for both buildings. The damping matrix $\mathbf{C}_d$ is given by:

$$\mathbf{C}_d = \begin{bmatrix} c_d & & & & \\ & \ldots & & & \\ & & c_d & & \\ & & & \ldots & \\ & & & & c_d \end{bmatrix} \tag{22}$$

The damping matrices of the corresponding MPD systems are equal to $\mathbf{C}_1 = \mathbf{C}_{I1} + \mathbf{C}_d$ and $\mathbf{C}_2 = \mathbf{C}_{I2} + \mathbf{C}_d$.

The seismic response of the coupled system is analysed considering the following normalized parameters: mass ratio $\rho = m_1/m_2$, and fundamental period ratio $\Omega = \omega_{1n,1}/\omega_{2n,1}$, with $\omega_{1n,1}$ and $\omega_{2n,1}$ being the first natural undamped frequencies of vibration of the reference structure (Building 1) and the support structure (Building

2), respectively. The corresponding periods of vibration are indicated as $T_{1n,1}$ and $T_{2n,1}$. The analyses are conducted varying the key parameters within the ranges reported in Table 2.

Table 2: Ranges of the key parameters considered in the parametric analysis.

	Total number of storeys N (Period $T_{1n,1}$)	Mass ratio ρ	Frequency ratio Ω	Normalized viscous damping ratio ξ_d
Range	5 ($T_{1n,1}$=0.35 s) 10 ($T_{1n,1}$=0.67 s) 20 ($T_{1n,1}$=1.30 s)	0.5; 1.0; 2.0	0.2 - 4.0 (step 0.1)	0.2 - 4.0 (step 0.1)

4.2. Displacement reduction factors under earthquake excitation

The response of the *N*-storey coupled systems under earthquake ground motion is investigated with the purpose of evaluating the trends of the damping reduction factors of peak roof displacements. For this purpose, the following damping reduction factors are introduced (subscript *r* stands for *roof*):

$$\eta_{r,1}\left(\xi_d\right)=\frac{u_{roof\,1,\max,\xi_d}}{u_{roof\,1,\max,\xi_d=0}} \tag{23}$$

$$\eta_{r,2}\left(\xi_d\right)=\frac{u_{roof\,2,\max,\xi_d}}{u_{roof\,2,\max,\xi_d=0}} \tag{24}$$

$$\eta_{r,MPD1}\left(\xi_d\right)=\frac{u_{roofMPD1,\max,\xi_d}}{u_{roofMPD1,\max,\xi_d=0}} \tag{25}$$

$$\eta_{r,MPD2}\left(\xi_d\right)=\frac{u_{roofMPD2,\max,\xi_d}}{u_{roofMPD2,\max,\xi_d=0}} \tag{26}$$

$\eta_{r,1}$ and $\eta_{r,2}$ are the reduction factors of the peak roof displacements for the reference structure (Building 1) and the support structure (Building 2), respectively; while $\eta_{r,MPD1}$ and $\eta_{r,MPD2}$ are the reduction factors of the corresponding MPD systems, namely MPD1 and MPD2. It can be noted that $u_{roof\,1,\max,\xi_d=0}=u_{roofMPD1,\max,\xi_d=0}$ and $u_{roof\,2,\max,\xi_d=0}=u_{roofMPD2,\max,\xi_d=0}$.

Figure 16 provides the curves of $\eta_{r,1}$ and $\eta_{r,2}$ vs ξ_d, for the coupled 5-storey system with ρ =1.0 (e.g. buildings of same total mass) and for selected Ω values (0.2, 0.5, 1.5, 2 and 4). For comparison purposes, also the trends of η_{rMPD1} and η_{rMPD2} are provided.

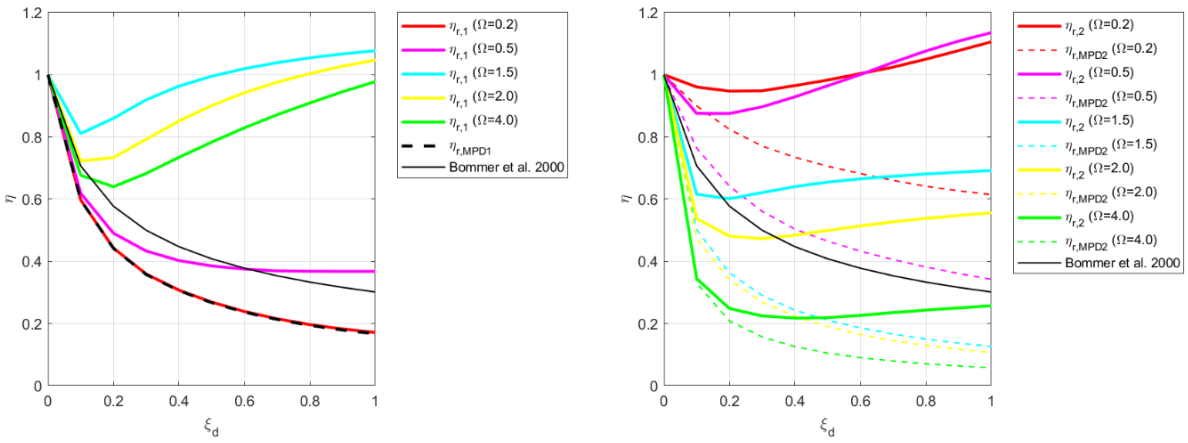

(a) (b)

Figure 16: Displacement reduction factors for N=5 and ρ=1.0: (a) $\eta_{r,1}$; (b) $\eta_{r,2}$.

Figure 17 provides the surfaces of $\eta_{r,1}$ and $\eta_{r,2}$ vs ξ_d and Ω, for the 5-storey, 10-storey and 20-storey systems with selected values of ρ (0.5, 1.0 and 2.0). It gives additional information about the dependence on the total number of storeys N (and therefore on the fundamental period $T_{1n,1}$) and mass ratio ρ. As for the one-storey systems, such dependence is not so remarkable.

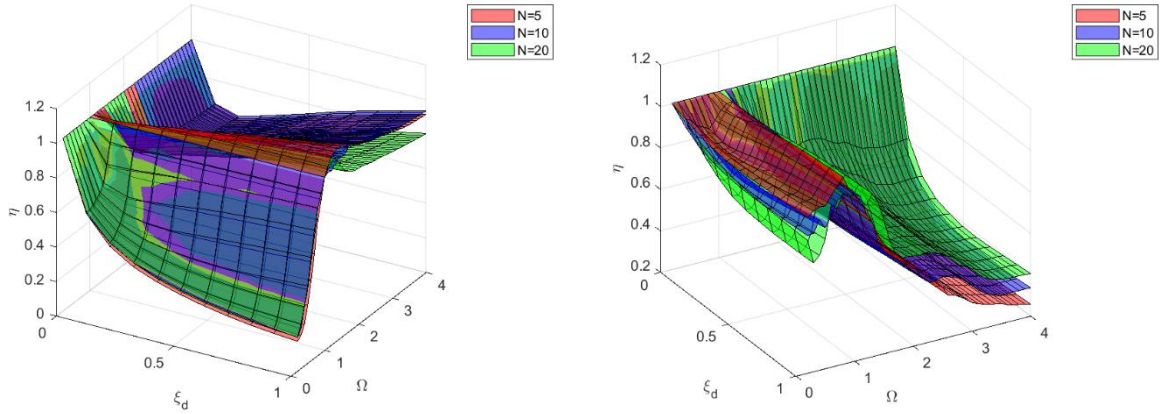

(a) (b)

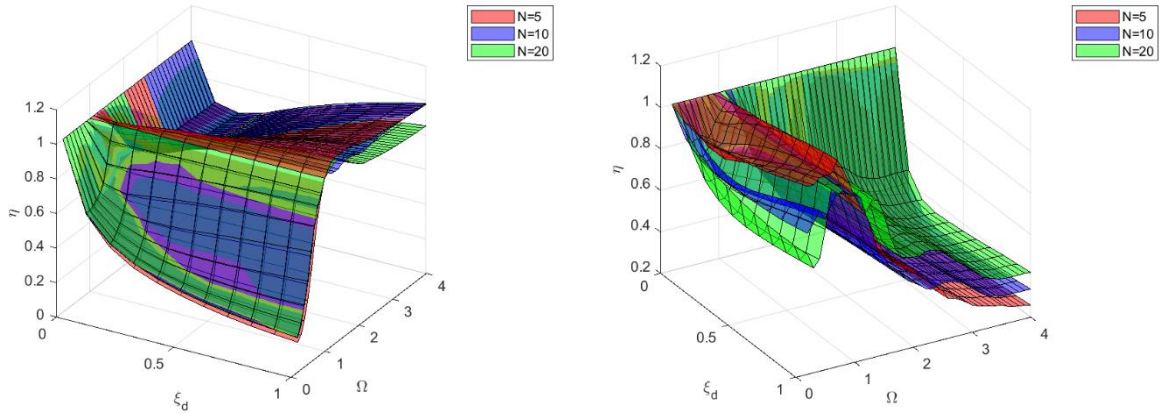

(c) (d)

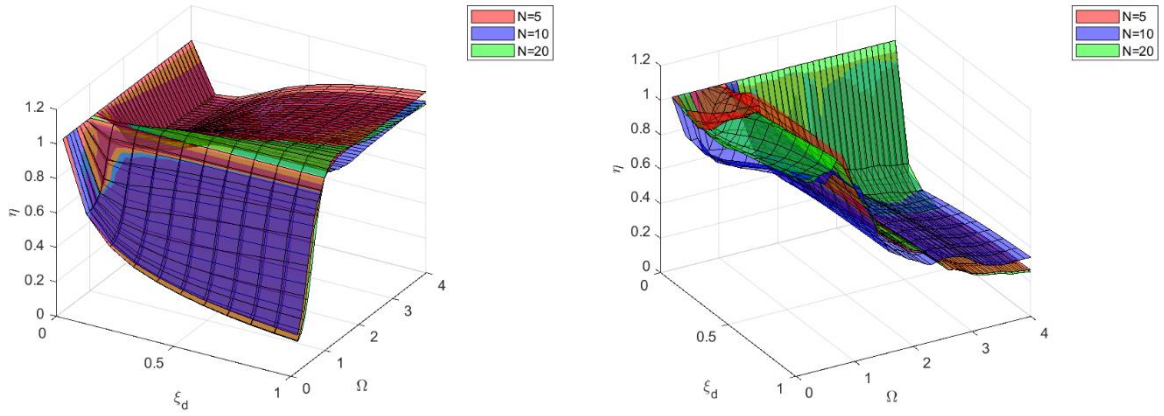

(e) (f)

Figure 17: Displacement reduction factors: (a) $\eta_{r,1}$ for ρ=0.5; (b) $\eta_{r,2}$ for ρ=0.5; (c) $\eta_{r,1}$ for ρ=1.0; (d) $\eta_{r,2}$ for ρ=1.0; (e) $\eta_{r,1}$ for ρ=2.0; (f) $\eta_{r,2}$ for ρ=2.0.

Visual comparison of the curves and surfaces for the uniform multi-storey buildings (Figures 16 and 17) with those related to the one-storey systems (Figures 11 and 12) allows to highlight that the trends of $\eta_{r,1}$ and $\eta_{r,2}$ are quite similar to those of η_1 and η_2 obtained for the one-storey systems. This suggests that the considered uniform multi-storey coupled systems are primarily governed by the "first" mode of vibration. For low Ω values (≤0.2), the $\eta_{r,1}$ curve is practically coincident with the $\eta_{r,MPD1}$ curve, thus indicating a large effectiveness of the dampers connection system in reducing the peak roof displacements for the entire range $0 \le \xi_d \le 1.0$. For $\Omega > 0.2$, the energy dissipation capabilities of the dampers connection system reduce and the minimum values of $\eta_{r,1}$ progressively increases with increasing values of Ω. For instance, for $\Omega = 0.5$, the minimum value of the $\eta_{r,1}$ curve (Figure 16a) is of around 0.4 and the corresponding ξ_d value ($\xi_{dr1}{}^*$) is around 0.2. On the contrary, as expected, the minimum values of the $\eta_{r,2}$ curves (Figure 16b) tend to increase as Ω values reduce.

The surfaces providing the trends of the minimum values of $\eta_{r,1}$ and $\eta_{r,2}$ (e.g. $\eta_{r1\min}$ and $\eta_{r2\min}$), with respect to the key parameters ρ, Ω and N, are shown in Figure 18.

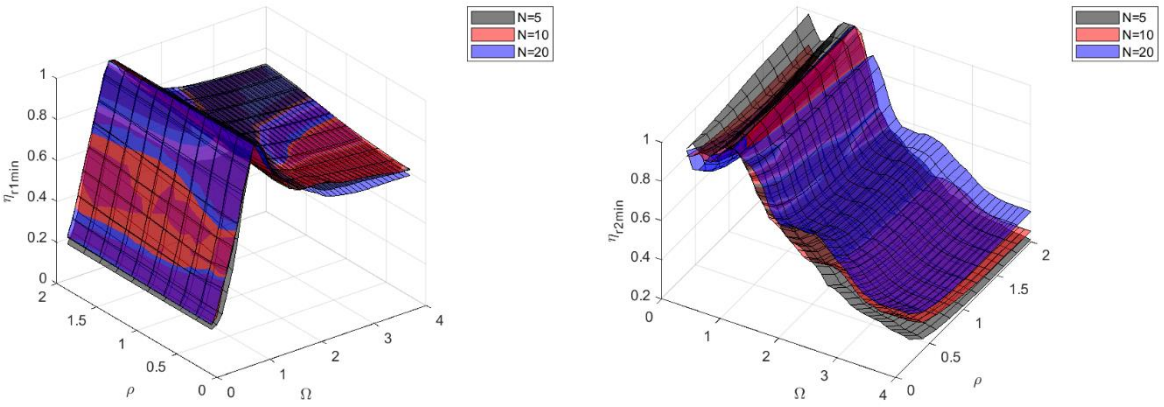

(a) (b)

Figure 18: (a) surfaces of $\eta_{r1\min}$; (b) surfaces of $\eta_{r2\min}$.

Again, the trends of $\eta_{r1\min}$ and $\eta_{r2\min}$ are similar to the ones obtained for the one-storey systems (Figure 15). Both $\eta_{r1\min}$ and $\eta_{r2\min}$ are mainly influenced by Ω, while their dependence on ρ and $T_{1n,1}$ is less significant. In detail, $\eta_{r1\min}$ first increases (almost linearly) for increasing values of Ω up to 1.0. Then, for $\Omega \geq 1.0$, a decreasing trend (almost hyperbolic) up to a value of around 0.6-0.7 at Ω = 4.0 is observed. Values of $\eta_{r2\min}$ oscillate between 0.7-1.0 for $\Omega \leq 1.0$. Then, for $\Omega \geq 1.0$, decreasing trends (almost hyperbolic) up to values around 0.2-0.4 at Ω = 4.0 are observed.

5. An estimation of the minimum damping reduction factors of peak roof displacements

5.1. Simplified upper and lower bound estimations

An estimation of the minimum damping reduction factor of the peak roof displacement of the reference building is proposed as a function of the fundamental frequency ratio Ω:

$$\eta_{1\min} = \begin{cases} \Omega & \text{for } 0.2 \leq \Omega \leq 1.0 \\ \dfrac{3-c}{3\Omega} + \dfrac{c}{3} & \text{for } 1.0 \leq \Omega \leq 4.0 \end{cases} \tag{27}$$

The functional form (linear branch for $0.2 \leq \Omega \leq 1.0$ followed by a descending branch with hyperbolic decay) assumed for $\eta_{1\min}$ (Eq. 27) is based on the results of the parametric analyses on both the one-storey and multi-storey buildings. Eq. 27 can be useful for a preliminary evaluation of the maximum effectiveness of the dampers connection system based on the fundamental dynamic properties of the two adjacent buildings. The values of parameter *c* can be calibrated from the results of the numerical simulations. Figure 19a displays Eq. 27 for different *c* values. Even though the detailed calibration of *c* values is beyond the scope of the present work, for the sake of providing upper and lower bound values, Figures 19b and c compare the estimations provided by Eq. 27 with the whole ensemble of the average results of the numerical simulations, including both the one-storey systems (Figure 19b) and multi-storey systems (Figure 19c). The legends of Figures 19b and c report the *c*-values providing upper and lower bound estimates.

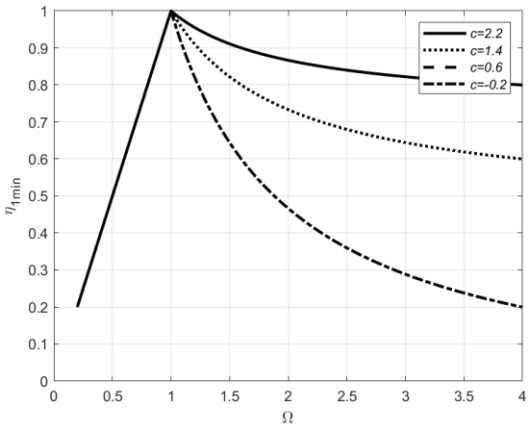

(a)

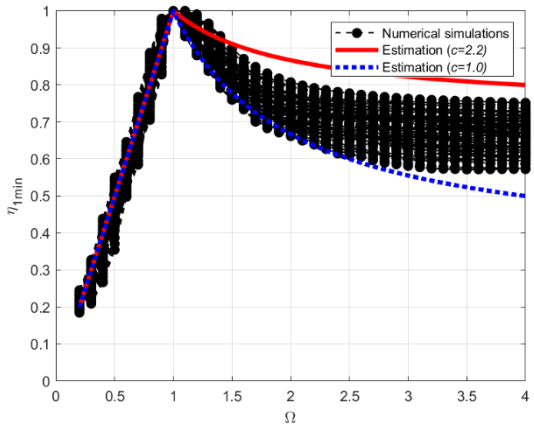

(b)

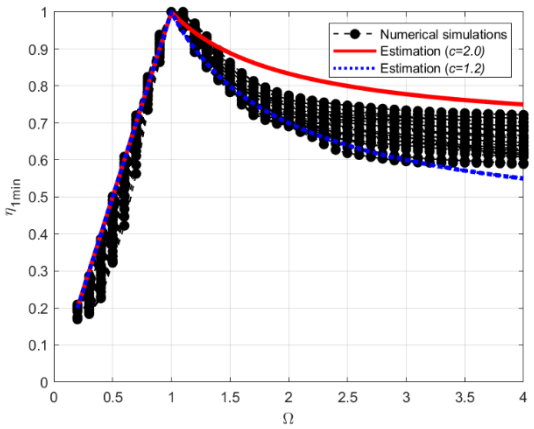

(c)

Figure 19: (a) $\eta_{1\min}$ for different c values; (b) upper and lower bound estimates of $\eta_{1\min}$ for one-storey systems; (c) upper and lower bound estimates of $\eta_{1\min}$ for multi-storey systems.

5.2. Applicative example

A two-bay six-storey steel moment-resisting frame is considered as the reference structure analysed as a case study. The columns and the beams are made by European HE and IPE profiles, respectively. The seismic weight of the main frame building is equal to W=2880 kN and the fundamental period of vibration is equal to T_1=1.25 s. It is supposed to connect all floors of the main building to four different support steel structures through linear fluid-viscous dampers with constant damping coefficient c_d at all floors. The resulting coupled systems are defined as follows (refer to Figure 20 for the cross section profiles and to Table 3 for the main system parameters):

- System C1: the main structure is connected to a very stiff braced frame support structure.
- System C2: the main structure is connected to a stiff braced one-bay frame support structure.
- System C3: the main structure is connected to an unbraced flexible one-bay frame support structure.
- System C4: the main structure is connected to an unbraced flexible three-bay frame support structure.

The diagonal braces of the support structures are made by circular hollow profiles (with diameter D=150 mm and thickness s=20mm). All frame elements have linear elastic behaviour. For comparison purposes, also the MPD system is considered. The MPD system is obtained connecting each floor of the reference frame with a fixed point through viscous dampers of equal damping coefficient c_d. Figure 20 displays the analysed systems, while Table 3 collects the values of their key parameters.

Table 3: Key parameters of the examined coupled systems.

System	Ω	ρ	ξ_d
C1	0.29	2	0.05-0.8
C2	0.78	2	
C3	2.34	2	
C4	2.54	0.5	

The seismic behaviour of the considered systems is investigated considering the El-Centro record as base input with the purpose of evaluating the reduction of the peak roof displacement of the reference frame for a specific earthquake record. The dynamic time-history analyses are developed using the software SAP2000 v.19 [31].

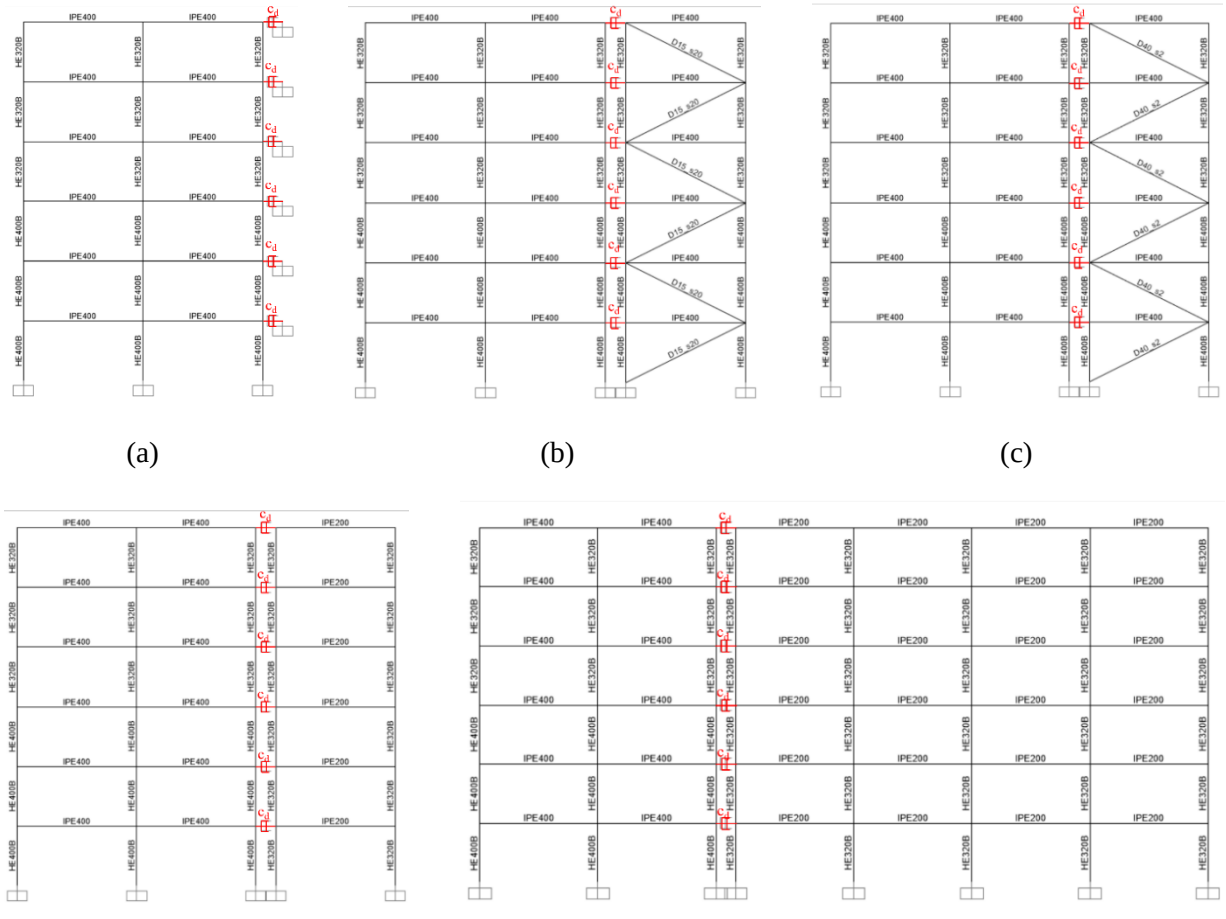

(a) (b) (c)

(d) (e)

Figure 20: The analysed systems: (a) MPD; (b) C1; (c) C2; (d) C3; (e) C4.

Figure 21 compares the peak roof displacement reduction factors η for the different systems as obtained from the numerical simulations. In detail, Figure 21a provides the trends of the damping reduction factor of the peak roof displacement as function of ξ_d.

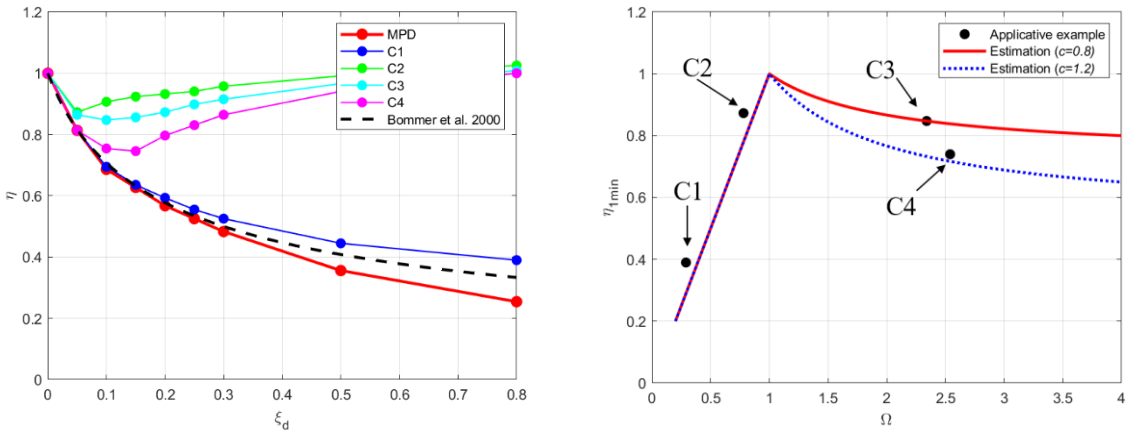

(a) (b)

Figure 21: Results from the applicative example. (a) η vs ξ_d; (b) η_{min} vs Ω.

As expected, for Ω=0.3 (system C1), the dampers connection system provides good energy dissipation capabilities, in line with those of the MPD system. Indeed, for large values of ξ_d significant reductions of the peak roof displacement are obtained (minimum values around 0.4). For the other three systems characterised by Ω values closer to and larger than 1.0 (systems C2, C3 and C4), the energy dissipation capabilities are reduced since the minimum values of η are between 0.74-0.87. The minimum damping reduction factors $\eta_{1\min}$ are displayed in Figure 21b and compared with the estimations given by Eq. 27. The estimations are able to reasonably well predict the obtained values. In detail, for the considered systems, values of the calibration parameter *c* are between 0.8 and 1.2.

Clearly, in the final design also the seismic response of the support structure has to be considered for the proper sizing of all structural members.

6. Conclusions

The paper provides an insight into the coupled dynamic behaviour of two adjacent multi-storey buildings (the one assumed as the reference structure, while the other as the support structure) connected through added viscous dampers. A wide parametric study has been carried out with the main purpose of evaluating the trends of damping reduction factors of peak displacements with respect to the key parameters of the system, namely frequency ratio Ω, mass ratio ρ, normalized damping coefficient ξ_d and fundamental period of the reference structure. The attention has been focused first on the minimal coupled dynamic system, namely the system composed by two Single-Degree-Of-Freedom systems connected by a viscous damper and therefore representative of a one-storey coupled system, and then to uniform multi-storey coupled systems.

The results of the analyses conduced on the one-storey coupled systems allow to draw the following conclusions:

- For certain combinations of key parameters (in particular, larger values of Ω), the limited values of one of the two damping ratio as obtained from complex frequency analysis indicate the limited effectiveness in energy dissipation of the coupled system independently from the amount of damping coefficient provided by the viscous damper.
- The trends of the frequency response functions of the coupled system evidence, for certain combinations of parameters, large dynamic amplifications even for large values of the damping coefficient.
- The trends of the damping reduction factors of the peak displacements of the masses of the two SDOF systems under earthquake excitation confirm that the maximum reduction (corresponding to the minimum values of the damping reduction factors) are highly dependent on the frequency ratio, the mass ratio and the fundamental natural frequency of the reference SDOF system: for low frequency ratios (less than 0.4) the reductions are close to those of the corresponding uncoupled damped SDOF systems; for larger frequency ratios, the maximum reductions rapidly reduce, strongly limiting the effectiveness of the dampers connection system.

The results of the analysis carried out on the uniform multi-storey coupled systems allow to draw the following conclusions:

- The trends of the damping reduction factors of the peak roof displacements are similar to those obtained for the one-storey coupled systems having the same key parameters: significant reductions of the peak floor displacements are observed for systems characterized by frequency ratios smaller than 0.4, while, for larger Ω values, the energy dissipation capabilities of the dampers connection

system drastically reduce and the maximum reductions of the peak roof displacements remain limited to 20% (corresponding to minimum damping reduction factors around 0.8).

- The analytical formula proposed to evaluate the upper and lower bound values of the minimum values of the damping reduction factor of the peak roof displacement can be useful in the preliminary design phase for a rapid assessment of the potential energy dissipation capabilities provided by the supplemental dampers connecting the two adjacent buildings.

Acknowledgements

Financial supports of Department of Civil Protection (DPC-Reluis 2019–2021 Grant—Research line WP15 "Code contributions for seismic isolation and dissipation'') is gratefully acknowledged.

References

[1] Moustafa, A., & Mahmoud, S. (2014). Damage assessment of adjacent buildings under earthquake loads. Engineering Structures, 61, 153-165.

[2] Naserkhaki, S., Aziz, F. N. A., & Pourmohammad, H. (2012). Earthquake induced pounding between adjacent buildings considering soil-structure interaction. Earthquake Engineering and Engineering Vibration, 11(3), 343-358.

[3] E. Rosenblueth, R. Meli, The 1985 Earthquake: Causes and effects in Mexico City, Concr. Int. ACI 8 (5) (1986) 23–36.

[4] Kasai, K., &Maison, B. F. (1997). Building pounding damage during the 1989 Loma Prieta earthquake. Engineering structures, 19(3), 195-207.

[5] J.E. Luco, F.C.P. De Barros, Optimal damping between two adjacent elastic structures, Earthquake Engineering and Structure Dynamics 27 (7) (1998) 649–659.

[6] Y.L. Xu, Q. He, J.M. Ko, Dynamic response of damper-connected adjacent buildings under earthquake excitation, Engineering Structures 21 (2) (1999) 135–148.

[7] W.S. Zhang, Y.L. Xu, Vibration analysis of two buildings linked by Maxwell model-defined fluid dampers, Journal of Sound and Vibration 233 (5) (2000) 775–796.

[8] T. Aida, T. Aso, K. Kakeshita, T. Takiuchi, T. Fujii, Improvement of the structure damping performance by interconnection, Journal of Sound and Vibration 242 (2) (2001) 333–353.

[9] H.P. Zhu, Y.L. Xu, Optimum parameters of Maxwell model-defined dampers used to link adjacent structures, Journal of Sound and Vibration 279 (1–2) (2005) 253–274.

[10] J. Kim, J. Ryu, L. Chung, Seismic performance of structures connected by viscoelastic dampers, Engineering Structures 28 (2) (2006) 183–195.

[11] Bhaskararao, A. V., & Jangid, R. S. (2006). Seismic response of adjacent buildings connected with friction dampers. Bulletin of Earthquake Engineering, 4(1), 43-64.

[12] Bhaskararao, A. V., & Jangid, R. S. (2007). Optimum viscous damper for connecting adjacent SDOF structures for harmonic and stationary white-noise random excitations. Earthquake engineering & structural dynamics, 36(4), 563-571.

[13] Zhu, H. P., Ge, D. D., & Huang, X. (2011). Optimum connecting dampers to reduce the seismic responses of parallel structures. Journal of Sound and Vibration, 330(9), 1931-1949.

[14] Gattulli, V., Potenza, F., & Lepidi, M. (2013). Damping performance of two simple oscillators coupled by a visco-elastic connection. Journal of Sound and Vibration, 332(26), 6934-6948.

[15] Tubaldi, E., Barbato, M., & Dall'Asta, A. (2014). Performance-based seismic risk assessment for buildings equipped with linear and nonlinear viscous dampers. Engineering Structures, 78, 90-99.

[16] Tubaldi, E. (2015). Dynamic behavior of adjacent buildings connected by linear viscous/viscoelastic dampers. Structural Control and Health Monitoring, 22(8), 1086-1102.

[17] Kasagi, M., Fujita, K., Tsuji, M., &Takewaki, I. (2016). Effect of non-linearity of connecting Dampers on Vibration control of connected Building structures. Frontiers in Built Environment, 1, 25.

[18] Kandemir-Mazanoglu, E. C., & Mazanoglu, K. (2017). An optimization study for viscous dampers between adjacent buildings. Mechanical Systems and Signal Processing, 89, 88-96.

[19] Y.L. Xu, W.S. Zhang, J.M. Ko, Experimental investigation of adjacent buildings connected by fluid damper, Earthquake Engineering and Structural Dynamics 28 (6) (1999) 601–631.

[20] Yang, Z., Xu, Y. L., & Lu, X. L. (2003). Experimental seismic study of adjacent buildings with fluid dampers. Journal of Structural Engineering, 129(2), 197-205.

[21] Trombetti, T., & Silvestri, S. (2004). Added viscous dampers in shear-type structures: the effectiveness of mass proportional damping. Journal of Earthquake Engineering, 8(02), 275-313.

[22] Trombetti, T., & Silvestri, S. (2007). Novel schemes for inserting seismic dampers in shear-type systems based upon the mass proportional component of the Rayleigh damping matrix. Journal of sound and vibration, 302(3), 486-526.

[23] Castaldo P., De Iuliis M. (2014) Optimal integrated seismic design of structural and viscoelastic bracing-damper systems, Earthquake Engineering and Structural Dynamics, 43(12), 1809-1827.

[24] Silvestri, S., Gasparini, G., & Trombetti, T. (2010). A five-step procedure for the dimensioning of viscous dampers to be inserted in building structures. Journal of Earthquake Engineering, 14(3), 417-447.

[25] A.K. Chopra, Dynamics of Structures: Theory and Applications to Earthquake Engineering, 2nd Edition. Prentice Hall, Upper Saddle River, New Jersey, 2001.

[26] Liang, Z., & Lee, G. C. (1991). Damping of structures, Part 1. National Center for Earthquake Engineering Research, Technical Report NCEER-91-0004, State University of New York at Buffalo, Buffalo, NY.
[27] Cheng FY (2001) Matrix analysis in structural dynamics. CGC, Rolla Missouri
[28] Gasparini, D., &Vanmarcke, E. H. (1976). SIMQKE: A program for artificial motion generation. Department of Civil Engineering, Massachusetts Institute of Technology, Cambridge, MA.
[29] Ministero delle Infrastrutture e dei Trasporti (NTC) (2018) Norme tecniche per le costruzioni, Ministero delle Infrastrutture e dei Trasporti, Decreto Ministeriale del 17 gennaio 2018, Supplemento ordinario alla G.U. n. 42 del 20 febbraio 2018 (in Italian)
[30] Bommer, J. J., Elnashai, A. S., & Weir, A. G. (2000, January). Compatible acceleration and displacement spectra for seismic design codes. In Proceedings of the 12th World Conference on Earthquake Engineering (pp. 1-8).
[31] CSI, 2016. Analysis Reference Manual for SAP2000, ETABS, SAFE and CSiBridge.